Accepted Review for Journal of Chemical Technology & Biotechnology 18 May 2018

Developments in Electrode Design: Structure, Decoration and Applications of Electrodes for Electrochemical Technology[†]

Frank C. Walsh,* Luis F. Arenas and Carlos Ponce de León

Electrochemical Engineering Laboratory, Energy Technology Group, Department of Mechanical Engineering, University of Southampton, SO17 1 BJ, UK

* Correspondence to: f.c.walsh@soton.ac.uk; +44 (023) 8059 8752.

Abstract

The diversity of cell geometries and their use for electrochemical processing and energy conversion are concisely reviewed, updating earlier treatments, with an emphasis on an engineering approach to electrode design. Electrode size varies from several cm^2 in the laboratory to a total of hundreds of m^2 at industrial plant scale and currents can range from several nA at laboratory through many 100 kA in industry. Electrode materials include metals, conductive ceramics and polymers as well as polymer-metal or ceramic-metal composites. Area, electrocatalytic activity and functionality can be tailored by selecting an appropriate support structure-coating combination. The core structure of porous supports can be a foam, mesh or particulate bed while the surface can be enhanced by many techniques. Inspiration for electrode design can come from many sources, including biomimetics and technology transfer. Important aspects of electrodes include manufacture, electrochemical activity, active area, the possibilities of 3D and nanostructured surfaces, decoration and functionalisation, in addition to reasonable cost and adequate lifetime. The diversity of electrodes is illustrated by examples from the author's laboratory in the fields of inorganic and organic synthesis, environmental remediation of wastewaters, surface finishing of materials and energy storage/conversion. A forward look is made to potential future developments in electrochemical technology.

Keywords: electrochemical engineering; electrode area; electrosynthesis; energy storage; environmental treatment; porous electrode.

[†] Based on the lecture following the award of the 2017 Castner Medal of the Electrochemical Technology Group of the SCI. London, 31 October 2017.

Highlights

- The importance of electrodes in electrochemical technology is emphasised.
- The diversity of electrode scale is stressed.
- Methods for fabrication and surface modification are reviewed.
- Hybrid 3D porous electrodes and nanostructured surfaces are highlighted.
- Current and potential applications are illustrated by examples.

Contents

(Approx. 10,000 words, 62 references, 14 reactions/equations, 0 tables, 20 figures).

Nomenclature

A	Geometrical electrode area	cm^2
A_{XS}	Cross-sectional area of electrical conductor	cm^2
c	Concentration of electroactive species	mol cm^{-3}
C	Capacitance	F
C_s	Specific capacitance	F g^{-1}
E	Electrode potential	V
E_{CELL}	Cell voltage	V
$E_{e,CELL}$	Equilibrium cell voltage	V
F	Faraday constant	C mol^{-1}
G	Electrical conductance	S = ohm^{-1}
ΔG_{CELL}	Gibbs free energy change (for a cell reaction)	J mol^{-1}
I	Current	A
I_L	Limiting current density (due to mass transport control)	A cm^{-2}
j	Current density ($j = I/A$)	A cm^{-2}
j_o	Exchange current density	A cm^{-2}
k_m	Mass transfer coefficient	cm s^{-1}
l	Length of conductor	cm
n	Amount of material	mol
R	Molar gas constant	J K^{-1} mol^{-1}
R_e	Electrical resistance	ohm
t	Time	s
T	Temperature	K
v	Mean electrolyte velocity	cm s^{-1}
V	Volume	cm^3
w	Mass of active material	g
z	Electron stoichiometry	Dimensionless

Greek

α	Charge transfer coefficient	Dimensionless
η	Overpotential	V
ν	Kinematic viscosity of the electrolyte	$cm^2\ s^{-1}$
ρ_e	Electrical resistivity	$ohm^{-1}\ cm^{-1}$
θ	Current efficiency	Dimensionless

Subscripts

A	Anode
act	Activation control
C	Cathode
CELL	Cell
conc	Mass transport control
e	Equilibrium

Abbreviations

ABS	acrylonitrile butadiene styrene
BDD	boron doped diamond
CNC	computer numerical control
PPyr	polypyrrole
RVC	reticulated vitreous carbon
SEM	scanning electron microscope
TEM	transmission electron microscope
UV	ultraviolet

Introduction

Electrochemical cells have a classical history[1] which predates studies by Faraday, Volta and others in the early 1800s. Such cells have seen developments which continue into the future. It is not always appreciated, however, that electrochemical cells are used on a wide scale from microimplants in living systems through to industrial production of commodity chemicals on a tonnage scale.[2] Recent advances in materials, coating technology, electrode manufacture, computational simulation of electrochemical systems and an increasing demand for sustainable electrochemical processes, justify an update of this field.

Some general comments based on the experience of the authors are important:

1) Considering an anodic (or a cathodic) reaction or electrode alone is equivalent to 'the sound of one hand clapping', since cells are integrated devices necessitating use of both electrodes in contact with an electrolyte and an external circuit (Figure 1). Commonly, the electronically conducting electrodes are metallic or carbon although ceramic, polymeric and composite electrodes are increasingly important. The electrochemical cell is comprised of an anode and a cathode in contact with an electrolyte. The electrolyte is an ionic conductor and may be a) an aqueous solution or gel, b) a non-aqueous ('ionic liquid') solution, c) a molten salt or d) a solid state (polymeric or ceramic) ionic conductor. The cell may be undivided, with one electrolyte common to both electrodes, or divided by an ionically conductive material, typically a microporous polymer or ceramic or else an ion-exchange polymer.

2) The anode is the electrode at which oxidation of a reactant occurs at the interface between electrode and electrolyte via electron loss; at the cathode, electron gain leads to reduction. The net cell reaction is a corresponding redox process. The desired (or primary) electrode reactions

often have competition from secondary ones, resulting in a real charge capability below the ideal one.

3) As a whole, the cell has several notable features:

a) It is electrically neutral.

b) Electrical current flows bidirectionally, as cations and anions, in the electrolyte.

c) Electrical current flows unidirectionally, as electrons, e^-, in the external circuit.

d) The reactions take place locally at the electrode/electrolyte interfaces, resulting in a potential difference, E_{CELL}, in the outer circuit between the electrodes.

4) From the viewpoint of energy conversion, there are two distinctly different types of cell (Figure 2). Galvanic cells release energy spontaneously, while electrolytic cells require an energy supply in order to drive non-spontaneous reactions.

5) Electrode potential, *E*, is 'the double-edged sword of electrochemistry'. An appropriate value can provide good control of reaction rate and efficiency; unsuitable or poorly distributed potential can result in poor efficiency or selectivity, due to side reactions, a lower reaction rate or unsuitable product purity or morphology in the case of solid films.

6) The rate determining step is the slowest one and often readily measured in the laboratory but is only part of a sequence in the overall reaction.

7) In some cells, e.g., secondary batteries, an electrode is anodic for part of a cycle, such as during charge, then cathodic for another period when the direction of current flow reverses, e.g., during discharge. However, the polarity (+ or –) of the electrode is invariant.

8) Microstructured and nanostructured electrode surfaces do not always behave as higher surface area versions of flat electrode surfaces.

9) In the case of bipolar electrodes, one side of the structure is anodic while the other is cathodic.

10) The electrode reactions can involve a wide range of reactant and product species and phases, including ions, radicals, uncharged solvent molecules, solids, liquids, gases and colloidal dispersions.

11) Electrode reactions carried out in practical settings often involve concentrated, multicomponent electrolytes and irreversible redox couples. In contrast, much of the electrochemical theory found in textbooks has been developed for highly diluted, fully reversible redox couples.[3]

The themes of this work, which looks towards technological applications, include:

1) The diverse nature of electrodes, as shown by their form, material, area, scale and use.

2) Inspiration for the design of new electrodes and their surfaces comes from many sources.

3) Suitable technology transfer from other fields can be productive.

4) Engineering and science are an indivisible continuum needing and integrated treatment.

In this review, the properties, structure and surface decoration of electrodes are considered followed by illustration of diverse electrodes for applications including energy conversion and storage, electrosynthesis, mass transport studies, destruction of contaminants, recovery of metals, environmental treatment and drug delivery, using examples from the authors' laboratory.

Electrochemical cell design for technology

Cell thermodynamics

In order to achieve an economical and efficient operation, the maximum available energy of an electrochemical cell must be considered. At equilibrium, the Gibbs free energy, ΔG_{CELL}, for the overall cell reaction is associated to the electron stoichiometry, z, and the Faraday constant, F:

$$\Delta G_{CELL} = -zFE_{e,CELL} \quad (1)$$

Note that this energy is directly related to the thermodynamic cell potential, $E_{e,CELL}$. For galvanic cells, the electrochemical cell reaction has a negative ΔG_{CELL} and electrical energy is generated spontaneously, as in discharging batteries and fuel cells (Figure 2). In contrast, electrolytic cells, having a positive ΔG_{CELL}, require input of electrical energy to drive the electrochemical reaction, as in secondary batteries during charging, electrosynthesis and electrodeposition. Energy efficiency has a different meaning in each case. In electrolytic cells, the cell potential should be minimized, while in galvanic cells it should be maximized as far as possible.

According to the Gibbs-Stockholm IUPAC convention,[4] the cell voltage is expressed as the difference between the potentials of the right and left hand side electrodes in a cell diagram; at open-circuit under equilibrium conditions:

$$E_{e,CELL} = E_{e,R} - E_{e,L} \quad (2)$$

If the cathode is placed on the right hand side,

$$E_{e,CELL} = E_{e,C} - E_{e,A} \quad (3)$$

In practice, when a current, *I,* flows through the cell, its potential can be expressed as:

$$E_{CELL} = E_{e,CELL} - |\eta_{c,act}| - |\eta_{a,act}| - |\eta_{c,conc}| - |\eta_{a,conc}| - \sum|IR| \quad (4)$$

Each of the terms in the equation represent the contribution of different cell components. Here, $\eta_{c,act}$ and $\eta_{a,act}$ are the anodic and cathodic activation polarization demanded by the electrode reactions. Meanwhile, $\eta_{c,conc}$ and $\eta_{a,conc}$ are the concentration polarization terms for each reaction, which become relevant at higher current densities away from equilibrium. Large values in the activation polarization can be decreased by implementing active catalysts or higher process temperatures. Similarly, higher mass transport can be achieved by enhancing electrolyte flow/stirring at the electrode or by employing concentrated electrolytes.

The ohmic losses in the cell are given by the term *IR*, which covers the ionic (electrolytes, ion exchange membranes) and electronic (electrodes, current collectors, contacts) resistances of the cell components1. These losses waste energy in the form of heat and therefore should be minimised. Highly conductive electrodes and busbars, adequately thin, conductive membranes, and low resistance at the electrode/current collector interphases are practical necessities both in industry and in the laboratory. Due to their simplicity, such considerations are often overlooked. Resistance at direct electrical contacts can be minimized by employing clean, polished surfaces and an adequate level of mechanical force between them. At large scale, specialized soldering and welding are more common.

The rate of an electrode process

Perhaps the most inevitable principles in electrochemistry are Faraday's laws of electrolysis. They will describe the global rate of an electrode reaction by relating the electrical charge, q, flowing through a cell to the amount of material transformed, Δn, for a reaction involving the transfer of z electrons:

$$q = \Delta nzF \tag{5}$$

The Faraday constant, F is the charge per mole of electrons. In the previous expression, the electrical charge, q is the result of integrating a current over a time interval:

$$q = \int_{t1}^{t2} Idt \tag{6}$$

As a result, if the electrode is operating at a constant current for a time, t, and the concept of current efficiency, θ, is introduced, equation (6) becomes:

$$\theta I = \frac{\Delta nzF}{t} \tag{7}$$

θ is the fraction of current involved in the desired reaction and would be unity in an ideal case. In practice, it is often <1 due to the occurrence of secondary reactions at the electrode surface.

Up to here, the total cell current has been considered. However, the processes at the electrode surface are sensitive, instead, to the current density, *j,* which is the ratio between the total current and the surface area of the electrode, *A*. The significance of knowing *A* for an electrode reaction cannot be stressed enough. The overall rate of chemical transformation of matter can be stated as:

$$\frac{\Delta n}{t} = \frac{\theta j A}{zF} \tag{8}$$

The overall rate of reaction in a cell will often be limited by the rate of one of the electrode reactions and it is important to realise which electrode becomes rate limiting first with increasing overpotential.

Current density and reaction control

In fact, depending on the current density value, three main forms of rate control may be achieved.[5] At low current densities, electron transfer prevails. In these conditions the current is extremely responsive to the potential; for an anodic process:

$$I = zFAkc \exp\left(\frac{\alpha z F \eta}{RT}\right) \tag{9}$$

where *k* is the rate constant, *c* is the reactant concentration, α is the electron transfer coefficient, η is the overpotential, *R* is the gas constant, and *T* is the temperature. As the current density increases, mass transport starts to play a role in the reaction rate, resulting in a combination of charge transfer and mass transport control, *i.e.,* mixed control regime. In reality, many large

cells operate under such conditions. This is particularly true in the case of porous electrodes, which usually display non-uniform current distributions at the electrode surface.

If the overpotential continues to increase, then full mass transport control is achieved, *i.e.*, the rate at which the redox species reaches or leaves the proximity of the electrode is the slowest step in the reaction. Under these conditions, a limiting current, I_L, is developed due to the restricted rate of convective-diffusion:

$$I_L = zFcAk_m \tag{10}$$

where k_m is the mass transport coefficient. At this point, the current becomes unaffected by increasing the potential until decomposition of the solvent takes place. High mass transport conditions are desirable and can be achieved by increasing electrolyte flow rate in flow cells or electrode angular velocity in disc or cylinder electrodes and by promoting turbulence and mixing by physical means such as non-conductive meshes or rough surfaces.

Electrode capacitance

In addition to those resulting from Faradaic electron transfer, electrical charges accumulate at the interface between the electrolyte and the electrode due to the presence of the electrochemical double layer and a capacitance, *C*:

$$C = \frac{q}{\Delta E} \tag{11}$$

where ΔE is the potential change. C is highly relevant when studying the electrosorption of species at the electrode, for instance, the well-known hydrogen underpotential deposition at platinum. Capacitance is directly proportional to the electrode surface area:

$$C = \frac{A \int j.dt}{\Delta E} \quad (12)$$

If the capacitance is too large, it can complicate the measurement of Faradaic currents. This is observed when performing cyclic voltammetry at elevated currents or when employing large electrodes. In some cases, capacitance can be used to estimate the surface area of an electrode.

Capacitance can be harnessed in several technologies, including water purification and energy storage.[6-9] Supercapacitors can supply large electrical charges in short time intervals, which has made them attractive for balancing the power grid. An important figure of merit for such devices is the specific capacitance, C_s, which is the capacitance per unit mass of active material w:

$$C_s = \frac{C}{w} \quad (13)$$

Electrochemical engineering aspects of electrodes and cells

Electrochemistry can extend much beyond the scale of common studies at the laboratory. The scope of electrochemistry covers anywhere from electrocatalyst studies at atomic or molecular sized species (involving several nA) to full scale commercial cell rooms with stacks operating at 10 kA-1000 kA. This is illustrated by Figure 3. Electrode size can be also extremely diverse. Laboratory electrodes might be <1 mm^2 to >10 cm^2 in size, not to mention microelectrodes. Pilot plant electrodes may be 100 cm^2 to >500 cm^2 in area while industrial pilot plant may involve electrodes of 0.1 m^2 to >1 m^2. Since scaling up electrochemical reactors usually involves grouping a number of electrodes in bipolar or monopolar stacks, industrial installations can involve total electrode areas from 10 m^2 to >>100 m^2.[10,11]

Electrodes are designed for a particular use, such as electrokinetic studies, determination of limiting currents, bulk electrolysis or continuous reactor operation.[2,5] Typically, the data obtained at the laboratory are expected to look clean and fit theory. In contrast, laboratory pilot-scale operation, perhaps in a flow cell, must establish process feasibility at high concentrations, the influence of operational variables, suitable cell components and materials, appropriate electrolyte flow conditions plus suitable models describing quantitative performance. The type of cell design is extensively considered elsewhere with respect to geometry, electrode shape and electrolyte flow/electrical connections.[2,12,13]

Mass transport of reactants/products and heat transport to/from the electrode become more important at large scale operation. Mass transport, should be sufficient to supply the electrode with the necessary reactant for an efficient operation. Furthermore, since the rate and selectivity of electrochemical reactions is dependent on temperature, thermal control also becomes necessary. Many redox reactions are exotermic by nature. Combined with the additional heat produced by the current flux via the Joule effect, active cooling might be required in the form

of heat exchangers. Thermal control plays an important role in ensuring the stability of materials and safety of the operation.

Important properties of electrodes

The following are prerequisite properties for practical electrodes:

1) Moderate costs, which might be achieved, *e.g.*, by a platinum catalyst coating on a lower cost substrate.

2) Good mechanical, thermal and chemical stability to ensure an adequate lifetime and freedom from corrosion.

3) Effective electrocatalysts to provide a low overpotential for the desired reaction.

4) A high electrical conductivity to realise low ohmic losses and a uniform current distribution.

Figure 4 indicates the range of electrical resistivity, ρ_e, encountered in electrode materials, the relationship to conductance, G, being:

$$G = \frac{1}{R} = \frac{A_{xs}}{\rho_e l} \qquad (14)$$

where l is the length of conductor having a uniform cross-sectional area, A_{xs}. It is important to select materials of reasonably low resistivity since short current paths are at odds with the high chemical resistance of materials such as titanium, which is further increased by the use of high surface area porous, 3D structures.

Diversity of electrode form, structure and scale

The diversity found in all aspects involving electrodes is illustrated in Figure 5. The electrode material can be a metal, polymer or composite. It may involve a 2D or 3D structure, be static or moving and be an uncoated single-piece or decorated by multiple particles. The typical electrode dimension can be m, cm, mm, μm or nm, depending on support material, type of surface finish and coating. Electrodes can be produced, imaged and studied by an increasingly wide range of techniques, from optical and SEM through X-ray computed tomography and synchrotron radiation (catalysts).

The importance of active electrode area, *A,* is readily appreciated by inspecting several fundamental expressions (Figure 6). Equation (8) indicates the importance of achieving a high current; if the current density is restricted, this necessitates increasing the active area, for example by using a 3D surface or porous structure. Such materials can offer a low pressure drop over the flow channel and moderate density. However, care must be taken to control the potential distribution to maintain a good current efficiency and, in the case of electrodeposited solids, suitable product morphology and purity.[2,10]

Figure 6 also indicates the importance of active electrode area for charge transfer, equation (9) or mass transfer, equation (10) controlled reaction conditions, the use of a greater active electrode area allows the current to be increased at a given reactant concentration and under particular reaction conditions. As indicated in equation (4), an increase in the current with electrode area will be accompanied by ohmic and kinetic losses, leading to a more negative cell voltage. In accordance with equation (12), an increase of active electrode area hence

electrical charge will result in a higher capacitance. While this presents problems in applying laboratory techniques such as cyclic voltammetry, one strategy for realising high specific capacitance in supercapacitors is the use of 3D surfaces such as microporous and nanostructured carbons.

Fabrication and imaging of electrodes

Trends in electrode materials include:

1) An increasing diversity of materials, rather than traditional metals and carbon; examples include conductive polymers,[14,15] such as polypyrroles or polythiophenes and ceramics, such as boron doped diamond and electrically conductive suboxides of titanium, including Ebonex.[16,17]

2) Modern ceramic-polymer composites, such as carbon fibre-polymer and metal-ceramic/polymer.

3) Deployment of mature coating techniques, such as vapour and plasma deposition, anodised and electrodeposited finishes.[18,19]

4) The introduction of nanostructured surfaces, with their high activity and area properties. Strategies to the fabrication of nanostructured electrodes can be additive (bottom up) or subtractive (bottom down) as indicated in Figure 7.

This review highlights electrochemical techniques for the production and surface modification of electrode structures but it is important to note that other approaches, which can be alternative or complementary, have joined the toolbox for realisation of modern electrochemical materials. Examples include electrostatic deposition and electrospinning of fibres. Ponce de León *et al.*

have utilised an electrostatically deposited Pd/Ir catalysed microfibrous carbon mat as a 3D cathode for peroxide reduction in a direct borohydride fuel cell.[20] Composite fibres of carbon nanotubes and hydrothermally synthesised titanate nanotubes incorporating biomaterials, such as chitosan, have been produced by electrospinning.[21]

The route to design and fabrication of cell bodies and electrode structures has been transformed by faster, digital-based fast prototyping, particularly computer numerical control (CNC) machining and 3D printing. Examples are considered in the following section. Furthermore, the continued development of classical imaging tools, such as scanning and transmission plus atomic force microscopy together with the introduction of newer techniques such as X-ray computed tomography[22] has done much to reveal the surface morphology of nanostructured surfaces and stimulate research in this area.

Modification and decoration of electrode surfaces

It is important to address both the benefits offered by modifying electrodes and the many methods used to achieve such modifications.

Strategies to achieving modified electrodes

Two approaches to achieving improved electrode surface properties by modifying existing structures are:

1) Hybrid porous, 3D electrodes. Reticulated vitreous carbon (RVC) foam electrodes have been extensively reviewed.[23,24] Possible ways of modifying such porous structures include: depositing high surface area, and active nanoparticles on the surface, combining the foam with

a fibrous or felt structure.[25] An example of the former is the deposition of gold nanospheroids, by sputtering, onto a nanoporous array of TiO_2 on a titanium foil, felt or mesh surface.[26,27] Approaches to the realisation of porous carbon foam electrode supports, offering a high (<97%) volumetric porosity to electrolytes together with an enhanced active area are shown in Figure 8.

2) Hybrid surface nanostructures. A hierarchical surface geometry comprised by 'tubes within tubes' is indicated in Figure 9.[26] This surface was prepared by incorporation of titanates into an anodised microporous TiO_2 array on a titanium foil via electrophoresis. Further studies have explored improved experimental conditions,[28] and the use of *in-situ* mechanical abrasion of the surface to promote insertion of nanotubes into the closed packed hexagonal porous array.[29]

The decoration of electrode surfaces

The surface of electrodes can be decorated with a variety of nanoparticles to confer enhanced activity and/or area. Useful techniques include sol-gel coating, chemical reduction of metal salts, electroless deposition and anodic or cathodic electrodeposition. Examples are considered in the section on applications.

In the case of electrochemical techniques, examples of deposited materials include:

1) Precious metals by galvanic reduction of metal salts, e.g., Pt and Ru catalysts on titanate nanotubes or Pt coatings on robust substrates, such as titanium mesh.[30,31]

2) A wide range of metals by immersion-, electroless- and cathodic deposition of e.g., Ni, Co, Pt and Sn or alloys such as Sn-Cu.[32,33]

3) Metal oxides, such as PbO_2 and MnO_2 by anodic deposition or by chemical oxidation from their salts.[34]

4) Composite metal-metal, metal-ceramic and metal polymer coatings by anodic and cathodic electrodeposition and anodising.[18,19]

3D printing and computational approaches to cell and electrode design

Traditionally, a workshop approach to flow cell production might involve machining of polymer sheet, typically 1-10 mm thick, to produce the required rectangular flow channel and manifolds, typically by milling. Such machining to remove material tends to be slow, costly and tedious, which has encouraged the use of moulding then CNC machining and fast prototyping using additive techniques, especially 3D printing, over the last 30 years.

Nowadays, cell design can be assisted by CAD, and computer modelling of the reaction environment, including electrolyte hydrodynamics, pressure drop, shunt currents ('leakage' or 'bypass' currents flowing through the electrolyte *around* rather than in an ordered fashion *through* each of the electrodes in a stack), together with concentration-, current- and potential distributions. Furthermore, fast prototypes of the digital designs can now be readily produced using 3D printing, enabling multiple, improved iterations of the cell. The prototypes can then be tested in the laboratory. However, it is essential to employ chemically and mechanically compatible materials as well as a suitable 3D printer, *i.e.*, capable of producing non-porous, impermeable components within the desired dimensional tolerances.

Recently, Ponce de León et al.[35] have reported the characterisation of a versatile, multi-purpose electrochemical flow cell manufactured via molten filament 3D printing. This acrylonitrile butadiene styrene (ABS) polymer cell could hold electrodes of 50 cm^2 and be used in divided or undivided, monopolar or bipolar configurations. Limiting currents for the reduction of $K_3Fe(CN)_6$ ions were determined at different electrolyte mean linear flow rates (up to 28 cm s^{-1}) at polished nickel electrodes. These currents were used to establish dimensionless group correlations describing the mass transport properties of the cell. Following a similar approach, local limiting current distributions at segmented electrodes were established for different 3D printed electrolyte manifolds in the flow cell.[36]

The possibility of producing fast prototypes of laboratory redox flow batteries has been demonstrated recently for the Zn-Ce flow battery.[37] The ability to quickly modify and manufacture the cell resulted in a much faster development process. Pressure drop measurements were performed to compare such cell with the FM01 laboratory reactor, showing a similar behaviour at the manifolds. The authors noted that employing 3D printing based on the melting of a polymer filament resulted in undesired porosity within the material and deformations due to residual thermal stresses. It was concluded that high resolution laser curing of resin was a more suitable technique for the printing of electrochemical flow cell components.

Developments in technology and the hardware of 3D printing have enabled an ever-wider range of solid materials to be realised, Examples include auxetic polymer foams having controlled pore shape, size and density.[38] Electrode structures available include metal fibres, foams and meshes, while diverse materials are possible using ink and laser wire/powder feed of raw material to the printer. In many cases, a post heating/curing stage can be used to consolidate the structure.

Developments in 3D printing have enabled the manufacture of 3D porous metal electrodes. A recent study has described the manufacture of laser metal stainless steel powder foams having controlled pore shape, size and density using a printer equipped with laser remelting of the surface under nitrogen.[39] The use of digital imaging software allowed visualisation, simulation and modification of structure prior to manufacture. Pressure drop across the structures was measured, in comparison to conventional metal foams, as a function of electrolyte flow rate, allowing permeability and friction factors to be established. Figure 11 shows some of the structures realised and their pressure drop *vs*. flow velocity characteristics in the range 2-14 cm s^{-1} for water at 25 ^{o}C passing through 10 mm diameter cylindrical discs of 5 mm length in a cylindrical flow channel. The SEM images in Figure 11a), b) and c) show the range of pore size realised while Figure 11d) show a CT image of rectangular pore, 20 ppi foam. The typical pressure drop *vs.* flow velocity characteristics of a range of porous bodies are shown in Figure 11e).

Nanostructured electrode surfaces

Despite the present fashion for nanostructured surfaces, the long history of nanostructured electrode surfaces is seldom appreciated. Platinised surfaces have long been used to achieve a high surface area, avoid polarisation effects and achieve improved reaction rates. The electrode surfaces of electrolyte conductivity probes are commonly platinised by electrodeposition following manufacture or renovation.[40] Early platinum black surfaces were used in electrolysers and fuel cells. Grove's 1842 letter to Faraday is summarised in Figure 12 and can now be viewed as a stack of bipolar, regenerative hydrogen-oxygen fuel cells.

Electrochemical techniques for the realisation of controlled surfaces by anodising and electrodeposition have been reviewed.[18,19] In favourable cases, it is possible to choose electrodeposition bath composition and control operating conditions such that nanostructured surfaces are directly deposited in a single step, one-pot, undivided cell, which facilitates industrial processing and scale-up. Nanostructured nickel has been electrodeposited from a chloride ion containing, acid sulphate, Watts nickel electrolyte.[41] The process was carried out at 100 mA cm^{-2} for 180 seconds after applying a surface pre-treatment at the same current density in 100 cm^3 dm^{-3} concentrated HCl and 240 g dm^{-3} $NiCl_2$ for 60 seconds.

The resulting surface had an average surface roughness of ca. 100 nm. Mass transport studies of ferricyanide reduction using 1 mmol dm^{-3} $Fe(CN)_6^{3-}$ in 1 mol dm^{-3} Na_2CO_3 at 25 ^oC in a rectangular flow channel, showed that the performance of the nanostructured electrode, compared to a flat nickel plate, was enhanced by a factor of 3-11 at linear flow velocities between 6 and 38 cm s^{-1}. Other examples of engineering electrodeposits from Watts nickel electrolytes have been highlighted elsewhere.[42]

Applications

Energy conversion

The use of a Pd-Ir catalysed carbon fibre mat as the cathode for peroxide reduction in a direct borohydride fuel cell has been mentioned in a previous section.[20] Various porous, 3D electrode structures have been used to oxidise borohydride in alkali for such cells.[43] In order to bring the concept of borohydride fuels cells closer to implementation, Abahussain *et al.* have recently carried out the characterization of the mass transport at diverse electrode geometries, such as plate and 3D mesh (fine and coarse), micromesh and felt.[44] All of the electrodes shown in

Figure 13, were manufactured Pt-Ir/Ti due to its high catalytic activity towards borohydride oxidation. The divided cell accommodated electrodes with projected areas of 9 cm^2 and operated in 0.01 mol dm^{-3} $NaBH_4$ in 2.0 mol dm^{-3} NaOH at 25 ^oC, the borohydride concentration facilitating mass transport studies. The felt electrode enhanced the limiting current by a factor of 100 in comparison to planar electrodes at an electrolyte velocity of 6 cm s^{-1}, although higher power densities were achieved by employing the fine mesh electrode at 100 mA cm^{-2}.

Similar 3D Pt/Ti electrodes, which are typically coated by a 3.5 μm thick electrodeposit of platinum, have been used for the positive electrode of a Zn-Ce hybrid redox flow battery.[45] Pt/Ti expanded mesh and in-house micromesh and felt were examined, their noble metal distribution studied by X-ray computed tomography.[31,46] Limiting current measurements were made for the reduction of Ce(IV) ions in an electrolyte containing 0.1 mol dm^{-3} Ce(IV) and 0.7 mol dm^{-3} Ce(III) in 4 mol dm^{-3} methanesulphonic acid at 25 ^oC. The current enhancement factor observed over 1-16 cm s^{-1} at the porous electrodes was between 15 and 20 for the mesh, between 52 and 62 for the micromesh stack and between 108 and 160 for the felt.[45] The volumetric mass transfer coefficient, k_mA_e was as high as 0.1 s^{-1} at a flow velocity of 12 cm s^{-1} for the felt, compared to a value of 0.0007 s^{-1} for the foil under similar conditions. The present authors also characterized the hydraulic characteristic of the same electrodes, as pressure drop over porous electrodes has significant consequences on the energy efficiency of electrochemical reactors.[47]

Environmental treatment

The use of electrochemical techniques for remediation of organic contaminants in wastewaters by anodic oxidation has greatly increased over the last 30 years.[48,49] For instance, 4-[4-(dimethylamino)phenylazo] benzenesulfonic acid [methyl orange] is commonly used as a textile dye. It has often been used as a model dye to characterise the performance of novel electrodes during its removal by oxidation reactions. Such processes can be readily scaled up and implemented in industry as a way to comply with environmental regulations.

De Vidales *et al.* studied the removal of methyl orange from wastewaters in a rectangular channel flow cell fitted with a nanoporous TiO_2 array coated titanium anode through a photoelectrocatalytic reaction,[50] examining the effect of electrode potential and electrolyte flow rate over its efficiency. The coating was prepared by anodising a titanium plate in 0.1 mol dm^{-3} NH_4F in aqueous ethylene glycol electrolyte at *ca.* 25 ^oC at 40 V for 100 minutes. A subsequent heat treatment in air for 100 min at 450 ^oC produced a photocatalytic surface under UV light. As shown in Figure 14a) and b), SEM imaging showed that the array coating consisted of 0.1 mm internal diameter titanate tubes. Under potentiostatic control at 1.5 V *vs*. Ag/AgCl, the decay of dye concentration with time was first order, as indicated in Figure 14c).

Recio *et al.* achieved highly crystalline, nanostructured, three-dimensional β-PbO_2 coatings by galvanostatic anodic deposition from electrolytes containing 1.0 mol dm^{-3} lead (II) methanesulfonate and 0.2 mol dm^{-3} methanesulfonic acid at 60 ºC and 20 mA cm^{-2}.[51] The matte grey deposits on the carbon substrate displayed adherence and high surface area. XRD analysis revealed that the crystal size was between 20-30 nm and AFM imaging showed uniform deposits with surface roughness between 255-275 nm. The authors studied several porous, 3D supports for the lead dioxide. Promising results were obtained with 275 cm^3 of 0.25 mmol dm^{-3} methyl orange in 0.05 mol dm^{-3} Na_2SO_4, at pH 3.0 and 22.5 ºC. An anodic Fenton process

with a large area carbon felt counter electrode and 0.2 mmol dm^{-3} Fe^{2+} in the electrolyte, as a catalyst, performed better than direct oxidation in the absence of ferrous ions. Quick and complete decolourisation was achieved in 60 minutes. Figure 15 indicates the performance of typical anodes. Those with a PbO_2/TiO_2 nanotubes coatings displayed higher activity towards the mineralization process compared to those modified only with PbO_2.

Zaidi *et al.* have studied a composite nanostructured 3D electrode involving PbO_2 particles on a decorated titanium felt surface anodised to form a nanotubular array of TiO_2.[52] The surface was treated at 25 ºC in methanesulfonic acid concentrations from 0.1 mol dm^{-3} to 5 mol dm^{-3} and 0.5 or 1 wt % NH_4F. A cell voltage of 30 V was applied between the felt and a graphite plate for 1 h. PbO_2 particles were anodically deposited for 6 h. over the nanotube array to produce well-dispersed coatings, the deposits appearing as cauliflower-like clusters, exhibiting α–PbO_2 phases. Its performance was recorded in solutions containing Reactive Black 5 [RB-5] azo dye. The electrochemical properties result from the generation of $^{\bullet}OH$ free radicals over the non-active Ti felt/TiNT/PbO_2 substrate while photocatalytic characteristics were related to the synergistic effect imparted by photo-induced holes and free electron acceptors. 99% decolourisation of RB-5 dye (as measured by visible absorption at 597 nm) was achieved after 60 min. anodic oxidation at the Ti felt/TiNT/PbO_2 anode. This coating was calcinated at 450 °C for 60 min in air, transforming the TiO_2 phase of the nanotubes into anatase, allowing 97% of RB-5 dye remediation within 30 min via photocatalytic degradation.

Coatings and surface finishes

Graves *et al.* have recently described a new method for the fabrication of metal nanowires for the electronics industry.[53] The method is based on electrodeposition using porous polycarbonate templates. First, a thin film of silver is sputtered on one side of the polycarbonate

foil. This is followed by the electroless deposition of copper up to a thickness of 300 - 500 nm. Acetone is then used to release the nanowires from the template mask. The authors demonstrated the process by preparing copper nanowires using controlled potential deposition. The procedure, shown in Figure 16A), can be used for other metals. A typical SEM of the tomography of the 'nanoforest' of wires is shown in Figure 16B), a close-up cross-section of the template/wire growth being provided in Figure 16C). This economical method can be used as an alternative to physical or chemical vacuum deposition for the production of nanowire surfaces.

The continued development of codeposition of materials by combining electroplating with electrophoresis of particles in a growing metal matrix[54] including nanoparticles[55] has facilitated a wide range of advanced tribological surfaces to be realised in engineering. Superhydrophobic surfaces, for instance, offer a high contact angle for water, ease of cleaning and less fouling. However, they usually have poor mechanical properties, which hinders their potential for application.

Recent work has sought to produce more robust surfaces. Zhao *et al.*[56] have recently described Ni-WC composite electrodeposits modified by stearic acid. These coatings retained their superhydrophobicity after a 450 cm long SiC abrasion test. Their maximum contact angle of water was *ca.* 164 deg with a sliding angle close to 0 deg. The authors found that varied surface morphologies could be obtained by controlling the concentration of WC nanoparticles in the electrolyte, the electrodeposition current density and mass transport, which was provided in the form of stirring. In essence, higher current density produced less roughness up to 8 A dm^{-2}, while a maximum concertation of WC particles was obtained from dispersions containing 20 g dm^{-3} at a rotation stirring speed of 800 rpm.

A super-hydrophobic, self-lubricating Ni-P-WS_2 coating prepared by electrodeposition has been described by He *et al.*[57] A superhydrophic Ni-P-WS_2 coating showing a low friction coefficient against steel was achieved by a one-pot process in a modified Watts nickel electrolyte containing 220 g dm^{-3} $NiSO_4 \cdot 6H_2O$, 30 g dm^{-3} H_3BO_3, 10 g dm^{-3} NaH_2PO_2, 12 g dm^{-3} citric acid and 45 g dm^{-3} $NiCl_2 \cdot 6H_2O$ at 60 °C. A hierarchical surface resulted of the adjustment of the particle size and CTAB surfactant concentration, displaying a water contact angle of *ca*. 160 °. Studies employing a tribometer showed that the WS_2 particles embedded in the <15 μm thick Ni-P coatings (3.6%wt) displayed a uniform dispersion due to the convection applied during the electrodeposition.

He *et al.* have also described a novel composite luminescent Ni electrodeposit incorporating blue-emitting phosphor particles for *in situ* wear detection. For this, a rare earth-based mixed metal oxide [$BaMgAl_{11}O_{17}:Eu^{2+}$] was dispersed in an aqueous electrolyte by using cationic surfactant and non-ionic surfactants and polyethylene glycol.[58] The effect of particle and additive concentration on the degree of phosphor content was analysed. Figure 17a) shows the cross-section of a one-layer coating, while Figure 17b) shows induced wear on this surface as revealed by fluorescent microscopy using light excitation at 450 nm. Figure 17c) shows a double composite coating and Figure 17b) the wear illuminated at 330 nm. It was found that coating luminescence could be maximized by employing a concentration of 5 g dm^{-3} of phosphor particles in the electroplating bath, rather than increasing the thickness of the deposit.

Zhou *et al.* have stressed the improved deposits achieved by dispersion of particles in electrolyte using high shear mixing, rather than the commonly used magnetic stirring.[59] The importance of this approach is illustrated in Figure 18, where the quality of electrolyte dispersion and deposit performance is considered for Ni-MoS_2 electrodeposits. Improved

dispersion of MoS_2 particles in the modified Watts nickel bath containing CTAB surfactant is indicated in Figure 18a). The effect of the dispersion method can be observed in Figure 18b) and Figure 18d), which show optical scans of the deposit morphology. The corresponding SEM images are shown in Figure 18c) and Figure 18e), respectively.

The controlled electrodeposition of Sn-Cu alloys from methanesulphonic acid electrolytes on porous, 3D carbon supports has been demonstrated by Low *et al*.[60] Figure 19a) shows the surface of a coating on RVC, which comprises a network of interconnected pores and provides a rigid, high surface area substrate.[22-24] Figure 19b) depicts a cross-section of the 4Sn46Cu50Bi alloy at the surface. Compressible carbon felts were also coated with the Sn-Cu alloy, as shown in Figure 19c). The morphology of the deposit can be appreciated in a closer view, Figure 19d). Such conductive carbon supports can be employed as anodes or cathodes in electrochemical flow cells due to their high hydraulic permeability. Furthermore, it is possible to produce multi-layered coatings with improved surface adhesion or enhanced functionality on the same substrates.

Drug delivery

The properties of electrodeposited conductive polymers can be harnessed for drug delivery systems. As described in a recent review,[61] a drug can be incorporated into a swelling film during the oxidation of a conductive polymer and subsequently released during the reduction, and shrinking, of the film under a controlled electrode potential. Alshammary *et al.* have demonstrated the possibility of delivering (4-isobutylphenyl)propanoic acid [ibuprofen] from an electrodeposited polypyrrole (PPy) film on a self-dissolving, biocompatible AZ31 Mg alloy.[62] Figures 20a) and 20b) show the anodic take-up of the drug during PPy formation in a salicylate electrolyte. Electrochemical and mechanical properties, deposit morphology,

thickness and drug release *vs*. time were studied in sodium salicylate solutions. The films containing the drug displayed a cracked surface with needle-like structures, as shown in Figures 20c) and 20d), respectively. In contrast, compact films prepared in the presence of salicylate only are compact, crack free and adherent. Similarly, the presence of the drug results in more plastic films, as shown by nano-indentation experiments. It was also shown that the formation of a Mg passivating layer during the oxidation of PPy could be overcome by concentrations of ibuprofen above 5×10^{-3} mol dm^{-3}. Up to 234 mg cm^{-2} of ibuprofen could be released in 15 min from 10 μm thick films. Avrami's equation described the overall kinetics of this process; see Figure 20e). A challenge for this drug-release concept is the uneven dissolution of the Mg substrate during ibuprofen release in 0.9% wt. NaCl. It is expected that thinner substrates or semi-protective intermediate layers could enable a homogeneous dissolution of the alloy.

22

10. Summary

1) The diversity of cell geometry and use in electrochemical processing and energy conversion are concisely reviewed with an emphasis on electrode design. The scale of electrode size varies from several cm^2 in the laboratory to hundreds of m^2 at full industrial scale.

2) Fundamental properties of electrodes, such as electrical resistivity and the importance of rate control are reviewed.

3) Electrochemical engineering aspects of electrodes, including reaction environment such as fluid flow, mass transport rates and thermal control are important in governing their properties in technological applications

4) Important developments to electrodes, such as modern, porous 3D structures, nanostructured surfaces, surface decoration and digital imaging and fabrication by 3D printing are illustrated by examples.

5) Current and developing applications for diverse electrode structures have been illustrated by examples from energy conversion, electrosynthesis, environmental treatment, coatings technology and drug delivery.

6) Developments in surface engineering coatings have included a range of composite electrodeposits involving one or more types of ceramic or polymer particles embedded into the growing metal matrix, examples including Ni-WC, Ni-S_2 and Ni-P-WC. Such coatings can confer properties such as enhanced wear resistance, lower friction, in-situ wear diagnosis and less wear.

7) For environmental treatment, approaches can be combined; an example is anodic photocatalytic degradation of organic dyes using photocatalysts, such as TiO_2, in nanostructured form and decorated with nanoparticulate electrocatalysts, such as PbO_2 spheroids.

8) One modern approach to controlled drug release is the use of a conductive polymer on magnesium alloy, in a self-driving, galvanic cell mode.

11. R & D needs and future developments

The following are important to the continued development of electrode materials:

1) Improved active area by surface decoration and modification of electrode supports.

2) Increased catalytic activity using nanostructured surfaces.

3) Tailored architecture to offer a gradation of electrode structure and composition with depth.

4) Hybrid structures to offer increased active area while maintaining benefits such as a high volumetric porosity for electrolyte flow.

5) Integrated use of digital imaging, computational software and fast prototyping manufacturing techniques to realise controlled, complex structure, composition and architecture for specific applications.

Future developments in these fields might build on past achievements to realise:

1) Electrically stimulated CT during medical operations, combining high resolution imaging with dynamic electrochemical activity.

2) Wireless control of battery recharging and UAVs for intelligent portable power and drones, encompassing self-diagnosis of cell or electrode condition and remote, dynamic control of electrodes/cells, offering a flexible and dynamic response.

3) Controlled drug release, *in-situ*, by remotely programmed triggering of bioelectrodes.

4) Intelligent, dynamic materials responding to environmental factors, using modified 3D printing technology in combination with digital imaging and computational design.

5) Highly efficient electrochemical reactors with tailored porous electrodes for electrosynthesis of chemicals, destruction of contaminants and energy storage.

Acknowledgements

FCW is grateful to the many students, academic colleagues and industrialists who have contributed to an integrated and cosmopolitan teaching, training, R&D, troubleshooting, scale-up and consultancy career. Particular thanks go to Prof Derek Pletcher. FCW first met many of his industrial and academic contacts at SCI Electrochemical Technology Group meetings, which provided a splendid opportunity for networking. Funding has been provided by industry, EU and EPSRC.

References

1. Ostwald W, Elektrochemie: Ihre Geschichte und Lehre. Leipzig; 1896. Electrochemistry: history and theory (2 volumes), translated by N.P. Date, Amerind Publ. Co., New Delhi (1980).

2. Pletcher D, Walsh FC, Industrial electrochemistry. 2nd edn. Chapman and Hall, London (1990).

3. Bard AJ, Faulkner LR, Electrochemical methods: Fundamentals and applications. 2nd edn. Wiley, New York (2000).

4. de Bethune AJ, The electrochemical thermodynamics of J. Willard Gibbs and the Stockholm Conventions. *J Electrochem Soc* **102**(12): 288C–292C (1955).

5. Pletcher D, A first course in electrode processes. 2nd edn. RSC Publishing, Cambridge (2009).

6. Porada S, Zhao R, Van der Wal A, Presser V, Biesheuvel PM, Review on the science and technology of water desalination by capacitive deionization. *Prog Mater Sci* **58**(8):1388–1442 (2013).

7. Conway BE, Electrochemical supercapacitors: Scientific fundamentals and technological applications. Springer (1999).

8. Béguin F, Frackowiak E, editors, Supercapacitors: Materials, systems, and applications. John Wiley & Sons (2013).

9. Yu A, Chabot V, Zhang J, Electrochemical supercapacitors for energy storage and delivery: Fundamentals and applications. CRC Press, Boca Raton (2013).

10. Walsh FC, Electrochemical technology for environmental treatment and clean electrochemistry: Electrode/membrane design and reactor characterisation. *Pure Appl Chem* **73**(12):1819–1837 (2001).

11. Wendt H, Kreysa G, Electrochemical engineering. Springer-Verlag, Berlin (1999).

12. Walsh FC, Reade GW, The design and performance of electrochemical reactors for efficient synthesis and environmental treatment. Part I Fundamental considerations. *The Analyst* **119**:791–796 (1994).

13. Walsh FC, Reade GW, The design and performance of electrochemical reactors for efficient synthesis and environmental treatment. Part II Typical reactors and their performance. *The Analyst* **119**:797–803 (1994).

14. Campbell SA, Smith JR, Li Y, Breakspear S, Walsh FC, Conducting polymer coatings in electrochemical technology. Part 1 – Synthesis and fundamental aspects. *Trans IMF* **85**(5):237–244 (2007).

15. Campbell SA, Smith JR, Li Y, Breakspear S, Walsh FC, Conducting polymer coatings in electrochemical technology. Part 2 – Application areas. *Trans IMF* **86**(1):34–40 (2008).

16. Smith JR, Walsh FC, Clarke RL, Electrodes based on Magnéli phase titanium oxides: the properties and applications of Ebonex materials. *J Appl Electrochem* **28**(10):1021–1033 (1998).

17. Wills RGA, Walsh FC, The continuing development of Magnéli phase titanium sub-oxides and Ebonex electrodes. *Electrochim Acta* **55**(22):6342– 6351 (2010).

18. Walsh FC, Ponce de León C, Bavykin DV, Low CTJ, Wang S, Larson C, The formation of nanostructured surfaces by electrochemical techniques: a range of emerging surface finishes. Part 1 Achieving nanostructured surfaces by electrochemical techniques. *Trans IMF* **93**(4):209–224 (2015).

19. Walsh FC, Ponce de León C, Bavykin DV, Low CTJ, Wang S, Larson C, The formation of nanostructured surfaces by electrochemical techniques: a range of emerging surface finishes. Part 2: Examples of nanostructured surfaces by plating and anodising with their applications. *Trans IMF* **93**(5):241–247 (2015).

20. Ponce de León C, Walsh FC, Bessette RR, Patrissi CJ, Madeiros MG, Browning DJ, Lakeman JB, Reeve RW, A direct borohydride-peroxide fuel cell using a Pd/Ir-coated microfibrous carbon cathode. *Electrochem Commun* **10**(10):1610–1613 (2008).

21. Dechakiatkrai C, Lynam C, Gilmore KJ, Chen J, Phanichphant S, Bavykin DV, Walsh FC, Wallace GG, Single-walled carbon nanotube/trititanate nanotube composite fibres. *Adv Eng Mater* **11**(7):B55–B60 (2009).

22. Arenas LF, Boardman RP, Ponce de León C, Walsh FC, X-ray computed micro-tomography of reticulated vitreous carbon. *Carbon* **135**:85–94 (2018).

23. Friedrich JM, Ponce de León C, Reade GW, Walsh FC, Reticulated vitreous carbon as an electrode material. *J Electroanal Chem* **561**:203–217 (2003).

24. Walsh FC, Arenas LF, Ponce de León C, Reade GW, Whyte I, Mellor BG, The continued development of reticulated vitreous carbon as a versatile electrode material: structure, properties and applications. *Electrochim Acta* **215**:566–591 (2016).

25. Castañeda LF, Walsh FC, Nava JL, Ponce de León C, Graphite felt as a versatile electrode material: properties, reaction environment, performance and applications. *Electrochim Acta* **258**:1115–1139 (2017).

26. Low CTJ, Ponce de León C, Walsh FC, A gold-coated titanium oxide nanotubular array for borohydride oxidation. *Electrochem Commun* **22**:166–169 (2012).

27. Zaidi SZJ, Harito C, Ponce de León C, Walsh FC, Anodising of titanium felt to produce TiO_2 nanotube arrays decorated with PbO_2 for RB-5 dye degradation. *In progress*.

28. Bavykin DV, Passoni L, Walsh FC, Hierarchical tube-in-tube structures prepared by electrophoretic deposition of nanostructured titanates into a TiO_2 nanotube array. *Chem Commun* **49**(62):7007–7009 (2013).

29. Martins AS, Harito C, Bavykin DV, Walsh FC, de Lanza MR, Insertion of nanostructured titanates into the pores of an anodised TiO_2 nanotube array by mechanically stimulated electrophoretic deposition. *J Mater Chem C* **5**(16):3955–3961 (2017).

30. Walsh FC, Bavykin DV, Torrente-Murciano L, Lapkin AA, Cressey BA, Synthesis of novel composite materials via the deposition of precious metals onto protonated titanate (TiO_2) nanotubes. *Trans IMF* **84**(6):293–299 (2006).

31. Arenas LF, Ponce de León C, Boardman RP, Walsh FC, Characterisation of platinum electrodeposits on a titanium micromesh stack in a rectangular channel flow cell. *Electrochim Acta* **247**:994–1005 (2017).

32. Low CTJ, Walsh FC, A review of developments in the electrodeposition of tin. *Surf Coat Technol* **288**:79–94 (2016).

33. Walsh FC, Low CTJ, A review of developments in the electrodeposition of tin-copper alloys. *Surf Coat Technol* **304**:246–262 (2016).

34. Li X, Pletcher D, Walsh FC. Electrodeposited lead dioxide coatings, *Chem Soc Rev* **40**(7):3879–3894 (2011).

35. Ponce de León C, Hussey W, Frazao F, Jones D, Ruggeri E, Tzortzatos S, McKerracher RD, Yang S, Wills RGA, Walsh FC. The 3D printing of a polymeric electrochemical cell body and its characterisation, *Chem Eng Trans* **41**:1–6 (2014).

36. Figueredo-Rodríguez HA, McKerracher RD, Ponce de León C, Walsh FC. Current distribution in a rectangular flow channel manufactured by 3D printing, *AIChE J* **63**(3):1144–1151 (2016).

37. Arenas LF, Walsh FC, Ponce de León C, 3D-printing of redox flow batteries for energy storage: A rapid prototype laboratory cell. *J Solid State Sci Technol* **4**(4):P3080– P3085 (2015).

38. Critchley R, Corni I, Wharton JA, Wood RJK, Walsh FC, Stokes KR. The preparation of auxetic foams by three-dimensional printing and their characteristics, *Adv Eng Mater* **15**(10):980–985 (2013).

39. Kaishubayeva N, Arenas LF, Walsh FC, Ponce de León C, Fluid pressure drop over 3D printed metal structures. *In progress.*

40. Reade GW, Ottewill GA, Walsh FC, Understanding electrical and electrolytic conductivity. *Trans IMF* **78**(2):89–92 (2000).

41. Recio FJ, Herrasti P, Vasquez L, C. Ponce de León C, Walsh FC, Mass transfer to a nanostructured nickel electrodeposit of high surface area in a rectangular flow channel. *Electrochim Acta* **90**:507–513 (2013).

42. Wang SC, Zhou N, Walsh FC. Diverse electrodeposits from modified acid sulphate (Watts nickel) baths, *Trans IMF* **94**(5):274–282 (2016).

43. Ponce de León C, Kulak A, Williams S, Merino-Jiménez I, Walsh FC, Improvements in the direct borohydride fuel cell using three-dimensional electrodes. *Catal Today* **170**(1):148–154 (2011).

44. Abahussain AA, Ponce de León C, Walsh FC, Mass-transfer measurements at porous 3D Pt-Ir/Ti electrodes in a direct borohydride fuel cell. *J Electrochem Soc* **165**(3):F198–F206 (2018).

45. Arenas LF, Ponce de León C, Walsh FC, Mass transport and active area of porous Pt/Ti electrodes for the Zn-Ce redox flow battery determined from limiting current measurements. *Electrochim Acta* **221**:154–166 (2016).

46. Arenas LF, Ponce de León C, Boardman RP, Walsh FC, Electrodeposition of platinum on titanium felt in a rectangular channel flow cell. *J Electrochem Soc* **164**(2):D57–D66 (2017).

47. Arenas LF, Ponce de León C, Walsh FC, Pressure drop through platinized titanium porous electrodes for cerium-based redox flow batteries. *AIChE J* **64**(3):1135–1146 (2018).

48. Bersier PM, Ponce de León C, Walsh FC, Electrochemical approaches to environmental treatment and recycling, in *Encyclopedia of life support systems*, eds. Feliu J, Martinez V, Climent V, EOLSS Publishers (2008).

49. Martínez-Huitle CA, Ferro S, Electrochemical oxidation of organic pollutants for the wastewater treatment: Direct and indirect processes. *Chem Soc Rev* **35**(12):1324–1340 (2006).

50. de Vidales JM, Saez LMC, Canizares P, Walsh FC, Rodrigo MA, de Arruda Rodrigues C, Ponce de León C, Photoelectrocatalytic oxidation of methyl orange on a TiO_2 nanotubular anode using a flow cell. *Chem Eng Technol* **39**(1):135–141 (2015).

51. Recio FJ, Herrasti P, Sires I, Kulak AN, Bavykin DV, Ponce de León C, Walsh FC, The preparation of PbO_2 coatings on reticulated vitreous carbon for the electro-oxidation of organic pollutants. *Electrochim Acta* **56**(14):5158–5165 (2011).

52. Zaidi SZJ, Harito C, Ponce de León C, Walsh FC, Decolourisation of Reactive Black-5 at an RVC substrate decorated with PbO_2/TiO_2 nanosheets prepared by anodic electrodeposition. *J Solid State Electrochem* (2018). *In press.*

53. Graves J, Bowker ME, Summer A, Greenwood A, Ponce de León C, Walsh FC, A new procedure for the template synthesis of metal nanowires. *Electrochem Commun* **87**:58–62 (2018).

54. Walsh FC, Ponce de León C, A review of the electrodeposition of metal matrix composite coatings by inclusion of particles in a metal layer: an established and diversifying coatings technology. *Trans IMF* **92**(2):83–98 (2014).

55. Low CTJ, Wills RGA, Walsh FC, Electrodeposition of composite coatings containing nanoparticles in a metal deposit. *Surf Coat Technol* **201**(1–2):371–383 (2006).

56. Zhao G, Li J, Huang Y, Yang L, Ye Y, Walsh FC, Chen J, Wang S, Robust Ni/WC superhydrophobic surfaces by electrodeposition. *RSC Adv* **7**:44896–44903 (2017).

57. He Y, Sun WT, Wang SC, Reed PAS, Walsh FC, An electrodeposited Ni-P-WS_2 coating with combined super-hydrophobicity and self-lubricating properties. *Electrochim Acta* **245**:872–882 (2017).

58. He Y, Wang SC, Walsh FC, Li WS, Heb L, Reed PAS, The monitoring of coating health by in-situ luminescent layers. *RSC Adv* **5**:42965–42970 (2015).

59. Zhou N, Wang S, Walsh FC, Effective particle dispersion via high-shear electrolyte mixing in electroplated nickel-molybdenum disulphide composite coating for improved tribological performance. *In progress.*

60. Low CTJ, Rotating electrodes: the electrodeposition of tin and tin-copper alloys. University of Southampton, United Kingdom, Doctoral Thesis (2007).

61. Alshammary B, Walsh FC, Herrasti P, Ponce de León C, Electrodeposited conductive polymers for controlled drug release: polypyrrole. *J Solid State Electrochem* **20**(4):839–859 (2015).

62. Alshammary B, Casillas N, Cook RB, Swingler J, Ponce de León C, Walsh FC, The importance of film structure during self-powered ibuprofen salicylate drug release from polypyrrole electrodeposited on AZ31 Mg. *J Solid State Electrochem* **20**(12): 3375–3382 (2016).

Figures

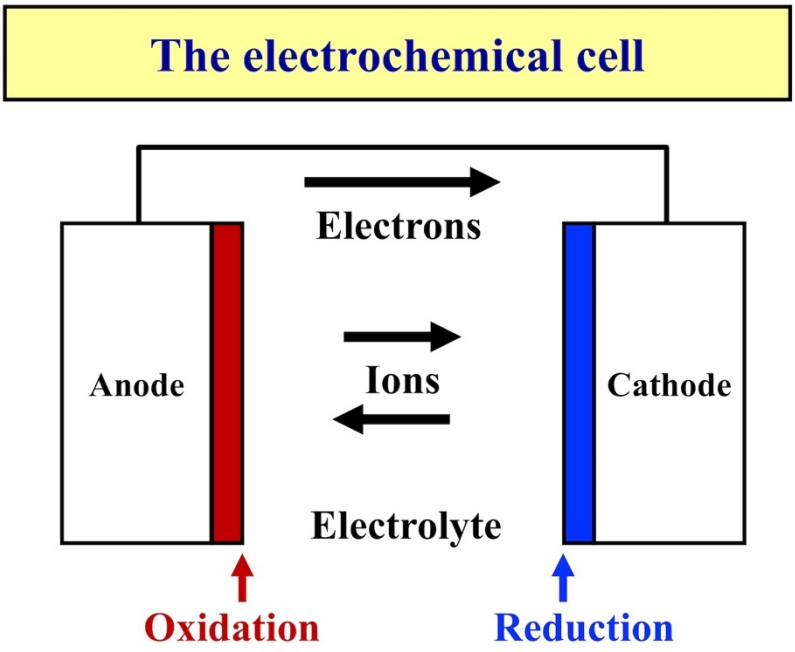

Figure 1. A schematic electrochemical cell, indicating the interfacial sites for reduction and oxidation together with the charge carriers involved.

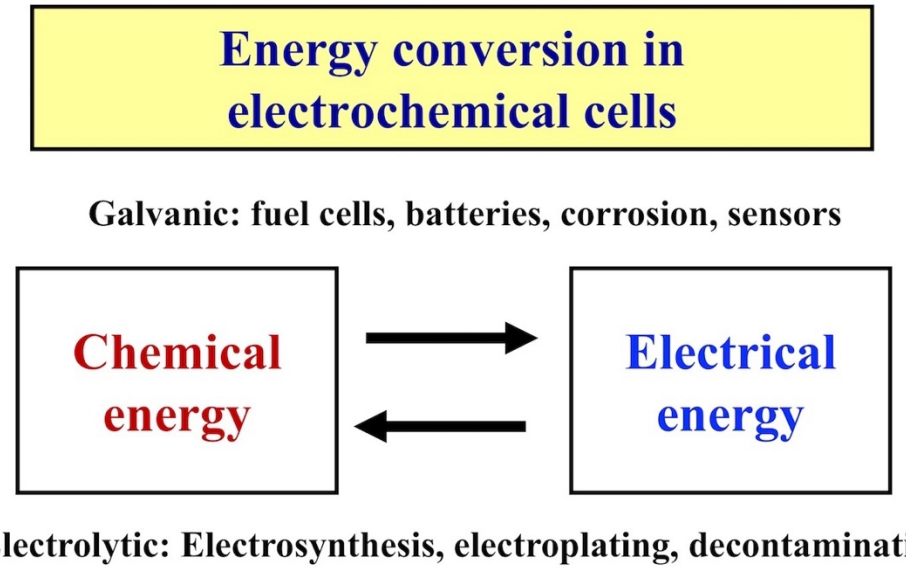

Figure 2. Galvanic and electrolytic cells, showing the direction of energy conversion with examples.

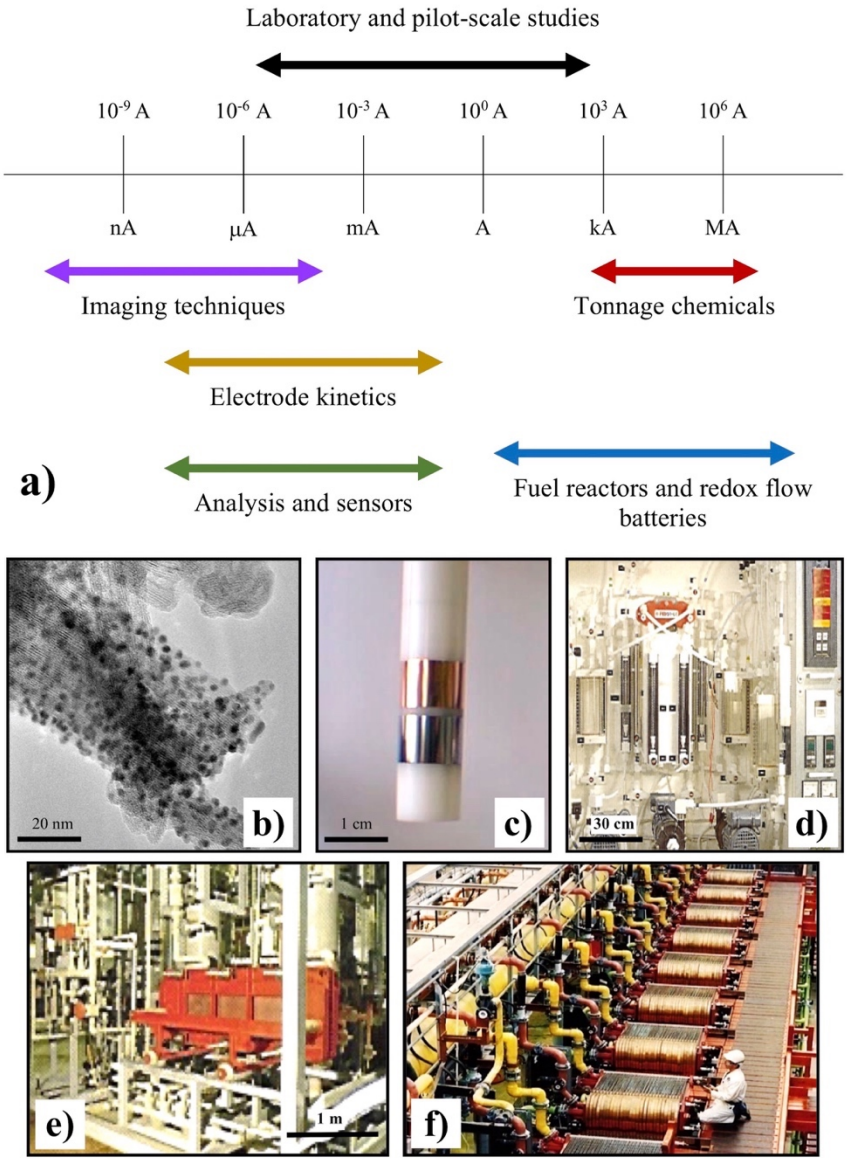

Figure 3. The diverse scale of electrochemical reactors, a) indicating electrode area and reactor current together with the typical range of subject areas; species involved and typical electrodes/cells involving b) electrocatalysts (nanostructured), c) laboratory electrodes (<1 mm^2 to >10 cm^2, d) laboratory pilot plant (100 cm^2 to >500 cm^2, e) industrial pilot plant (0.1 m^2 to >1 m^2) and f) industrial plant (10 m^2 to >>100 m^2).

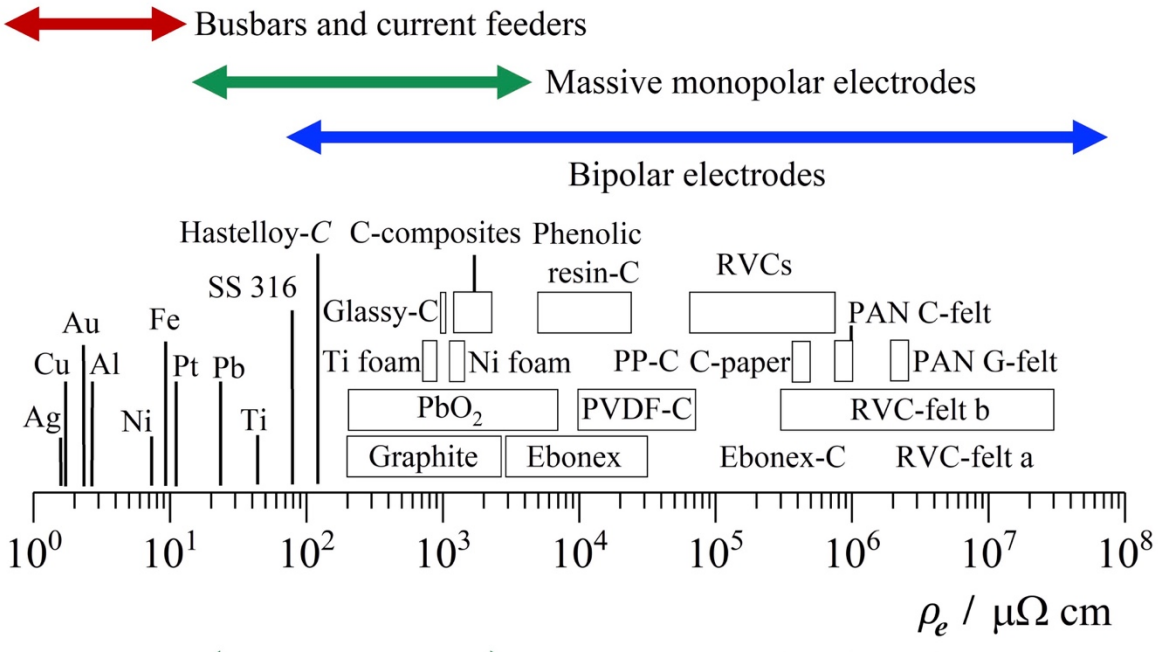

Figure 4. The electrical resistivity, ρ_e of electrode materials, showing a wide range of diverse materials and typical ranges for their deployment in electrochemical technology.

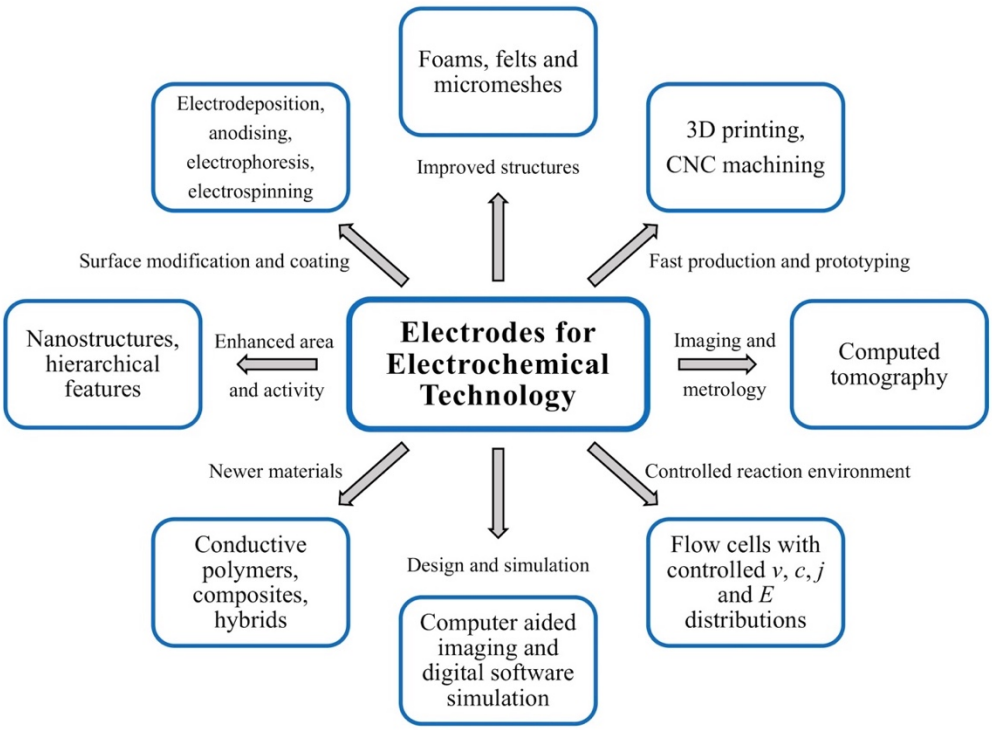

Figure 5. Possibilities for electrodes used in electrochemical technology, demonstrating a diversity of shapes, structures, materials, coatings, manufacturing methods and characterization techniques.

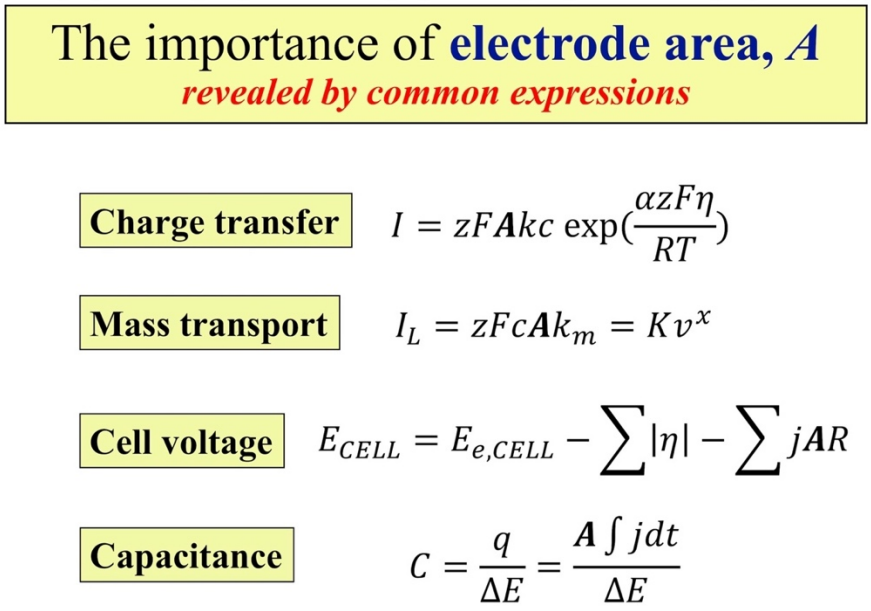

Figure 6. The importance of active electrode area, *A* is readily appreciated via fundamental expressions, involving equations (8), (9), (10) and (12).

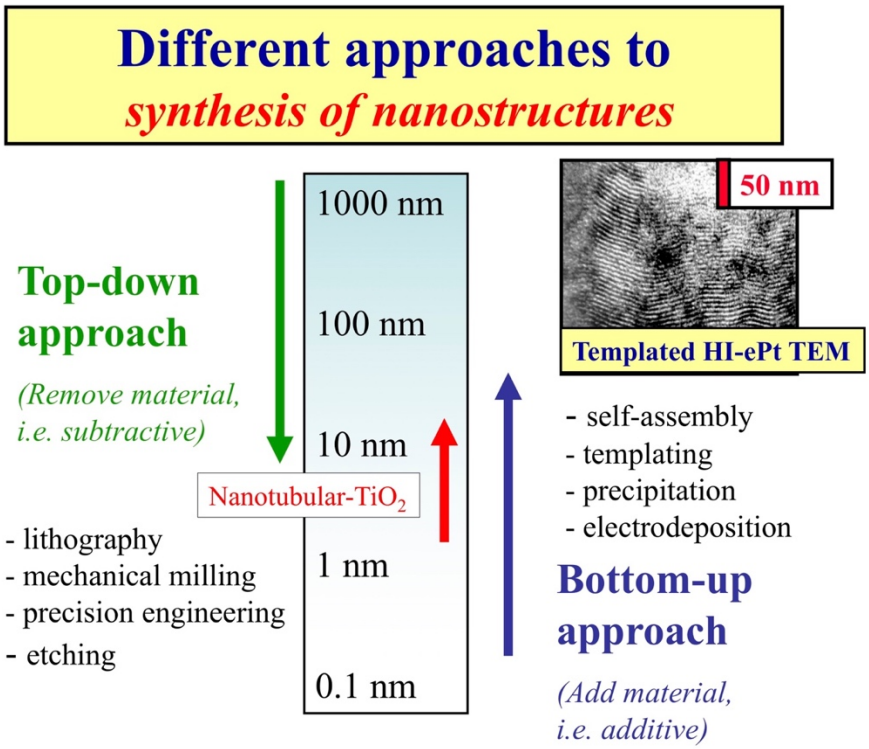

Figure 7. Strategies to achieve nanostructured surfaces, emphasising the difference between subtractive and additive techniques.

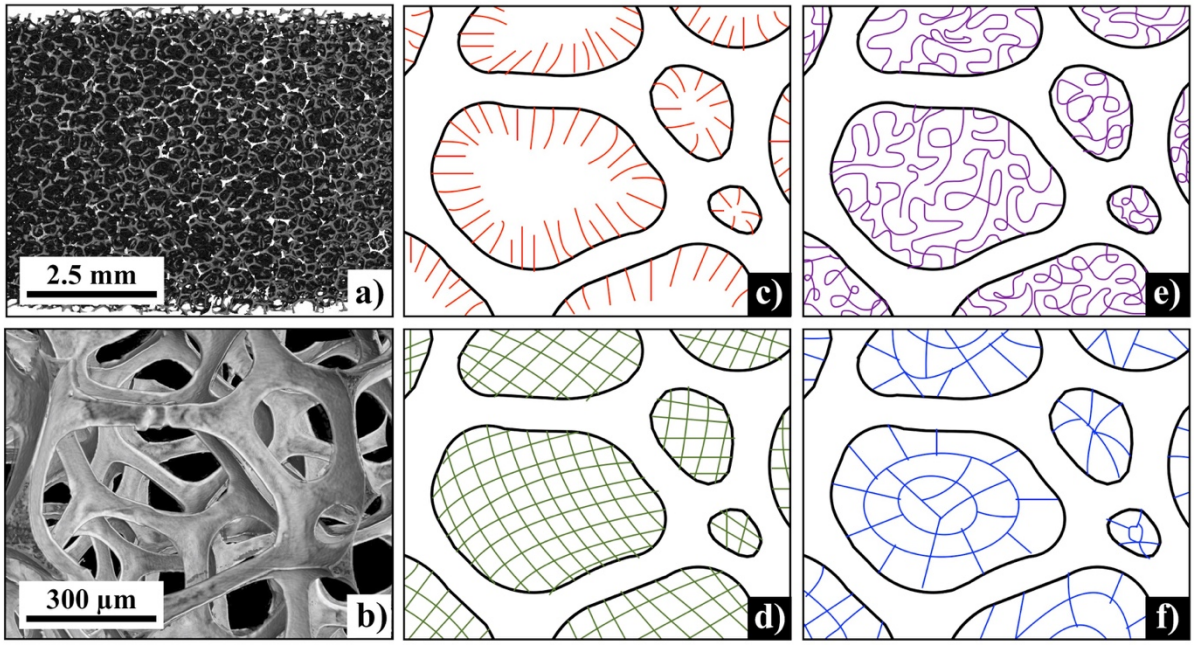

Figure 8. Hybrid 3D electrodes augmented by nanocatalyst structures. a) An X-ray computed micro-tomography image of 100 ppi RVC at resolution of 9.6 µm per voxel. b) A closer tomography view of the same material at a resolution of 1.3 µm per voxel, showing the structural features of the carbon foam. Methods to achieve hybrid porous RVC electrodes having higher active area by infilling pores: c) fibre infilling, d) infilling with felt nets, e) foam modified by felt, and f) modified with webs.

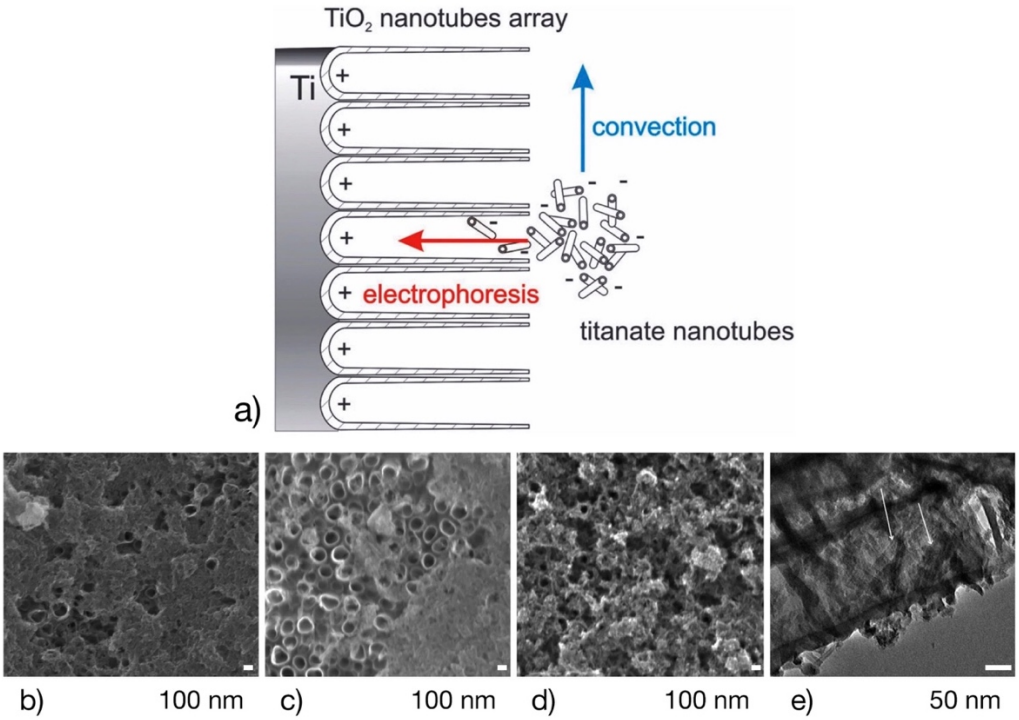

Figure 9. The realisation of a hierarchical, tube-in-tube surface geometry, using electrophoretic deposition into an anodised microporous surface. a). schematic of this methodology. SEM images of titanate nanotubes deposited on the surface of a TiO_2 porous array in an ethanol suspension at stirring rates of: b) 0 rpm, c) 50 rpm and d) 400 rpm. e) Cross-sectional TEM image of a large TiO_2 pore containing titanate nanotubes; stirring rate of 400 rpm. Adapted from Bavykin *et al.*,[28] with permission from The Royal Society of Chemistry.

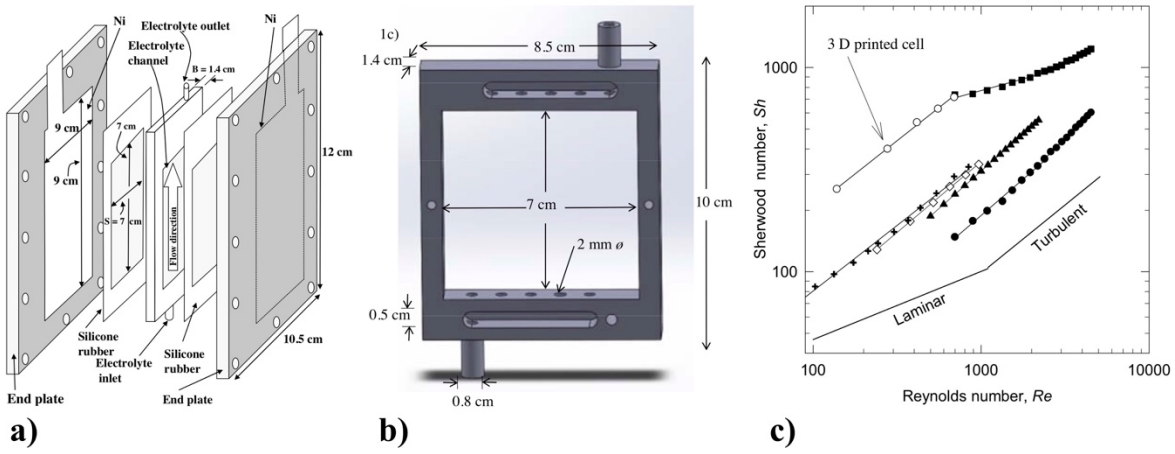

Figure 10. A 3D printed cell body for a laboratory rectangular channel flow cell. a) Schematic view of the 3D printed flow cell. b) Digital image of a 3D printed flow channel and c) Log-log plot of the correlation between *Sh* and *Re* obtained from the reduction of ferricyanide ions at nickel electrodes in different rectangular flow channel designs: ○) 3D printed flow cell, ◇) and ▲) FM01-LC pilot scale electrolyser, ✚) ElectroSynCell, ●) and ■) bulk and nanostructured Ni surfaces. The solid line represents the correlation for fully developed laminar and turbulent flow in a rectangular channel of the same dimensions. Adapted from Ponce de León *et al.,*[35] with permission from AIDIC/CET.

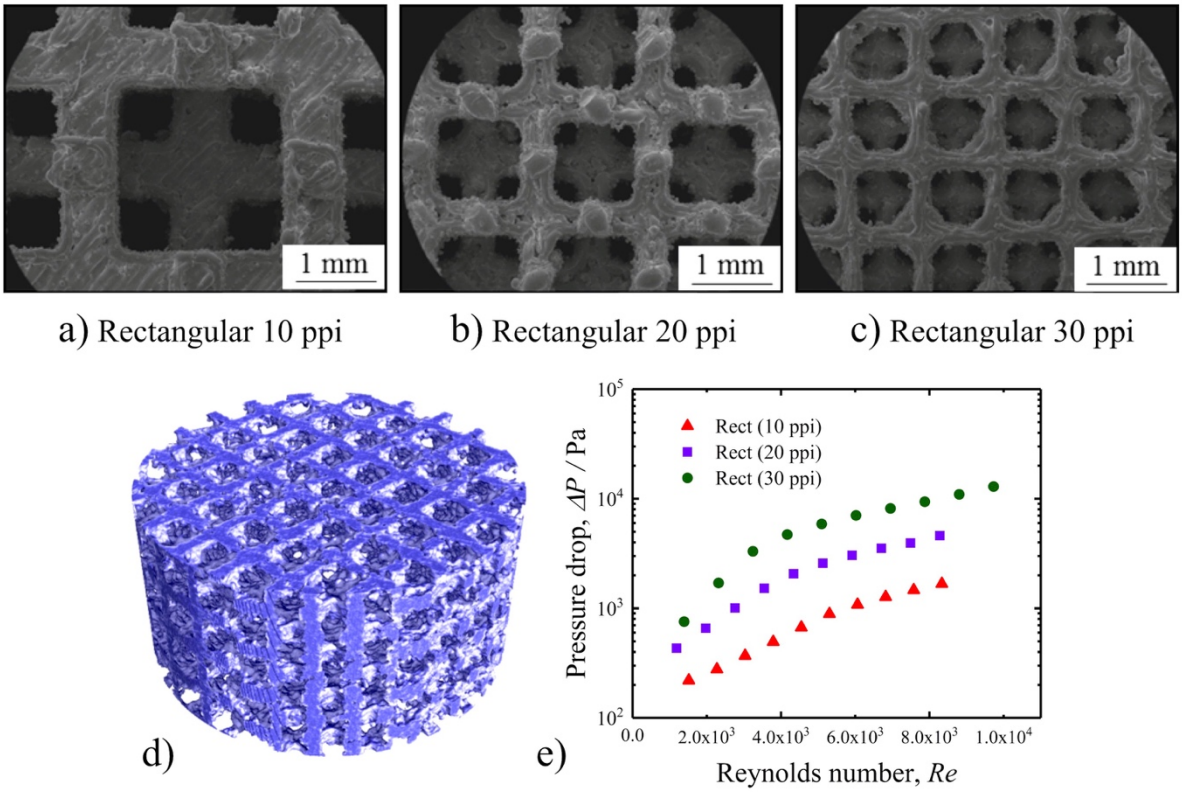

Figure 11. Stainless steel 3D printed porous structures manufactured by selective laser sintering of a metal powder precursor. a), b) and c) SEM images of various metal rectangular scaffolds with different pore sizes, d) X-ray computed tomography image of a 20 ppi structure, e) pressure drop of water at 25 ºC as a function of mean flow velocity for the range of printed porous bodies.

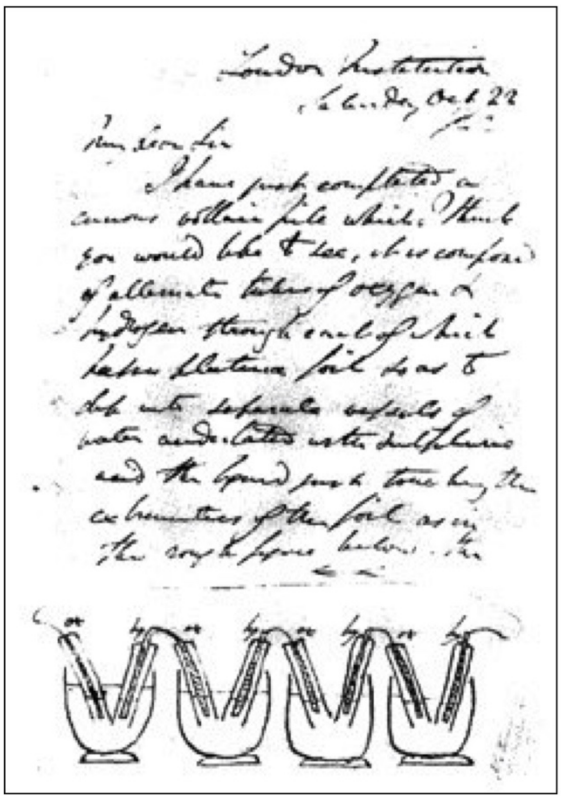

My Dear Sir,

I have just completed **a curious voltaic pile** which I think you would like to see. It is composed of alternate tubes of oxygen and hydrogen through each of which passes **platina** foil so as to dip into separate vessels of water acidulated with sulphuric acid, the liquid just touching the extremities of the foil as in the rough figure….

With 60 of these alternations, ***I get an unpleasant shock*** and decompose not only iodide of potassium but water so plainly that a continuous stream of thin bubbles ascends from each electrode…

I remain my dear sir
yours very sincerely

W.R. Grove

Figure 12. Grove's letter to Faraday in 1842 concerning the principles of a hydrogen-oxygen fuel cell/electrolyser, which can now be considered to indicate the strategy of operating a regenerative fuel cell/water electrolyser, using bipolar electrodes, having nanostructured surfaces, connected in electrical series.

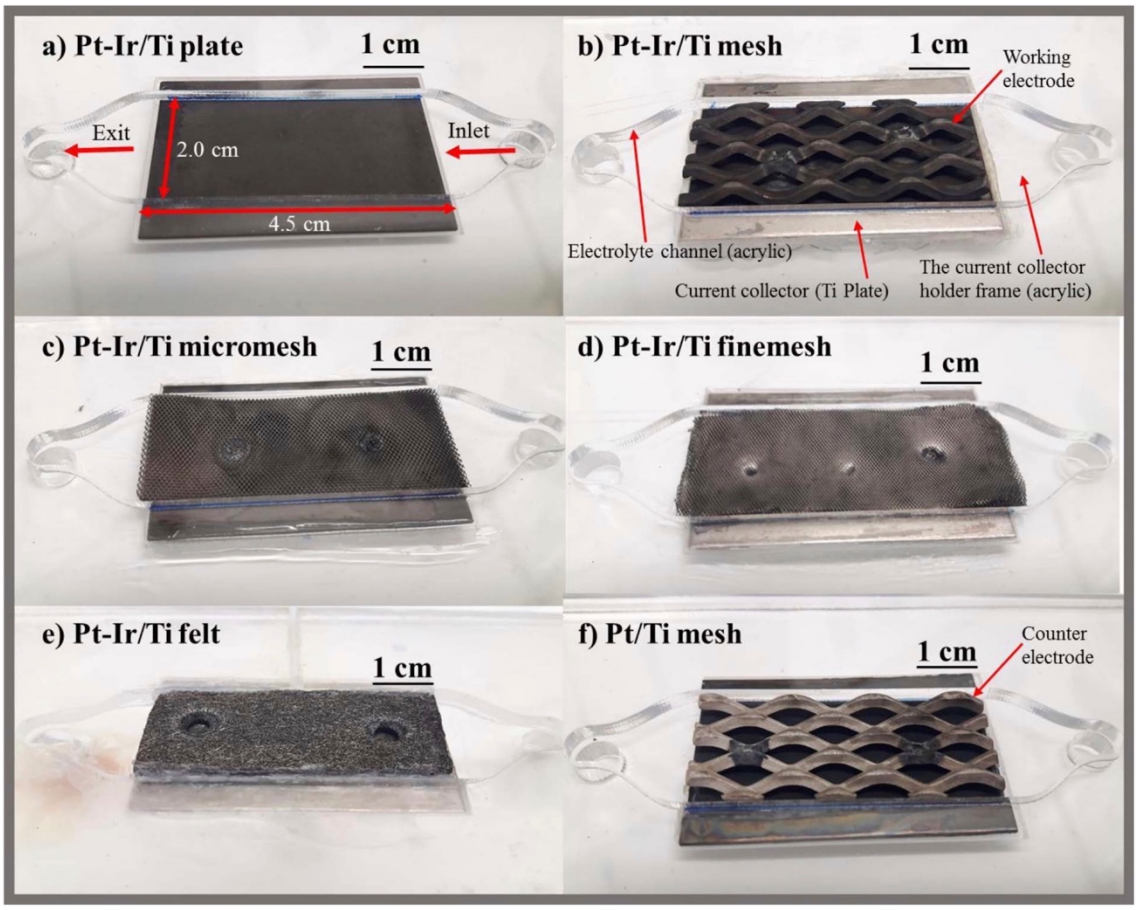

Figure 13. 3D platinum-iridium coated titanium anodes for use in a borohydride fuel cell along a platinized titanium cathode. a) Pt-Ir/Ti plate, b) Pt-Ir/Ti mesh, c) Pt-Ir/Ti micromesh, d) Pt-Ir/Ti fine mesh, e) Pt-Ir/Ti felt. f) Pt/Ti mesh cathodic counter electrode. All electrodes had geometrical projected areas of *ca.* 9 cm^2 and were spot-welded to a Ti current collector. Mean linear electrolyte flow velocities up to 16 cm s^{-1} were evaluated during mass transport studies for the oxidation of 0.01 mol dm^{-3} $NaBH_4$. Reproduced from Abahussain *et al.,*[44] with permission from The Electrochemical Society.

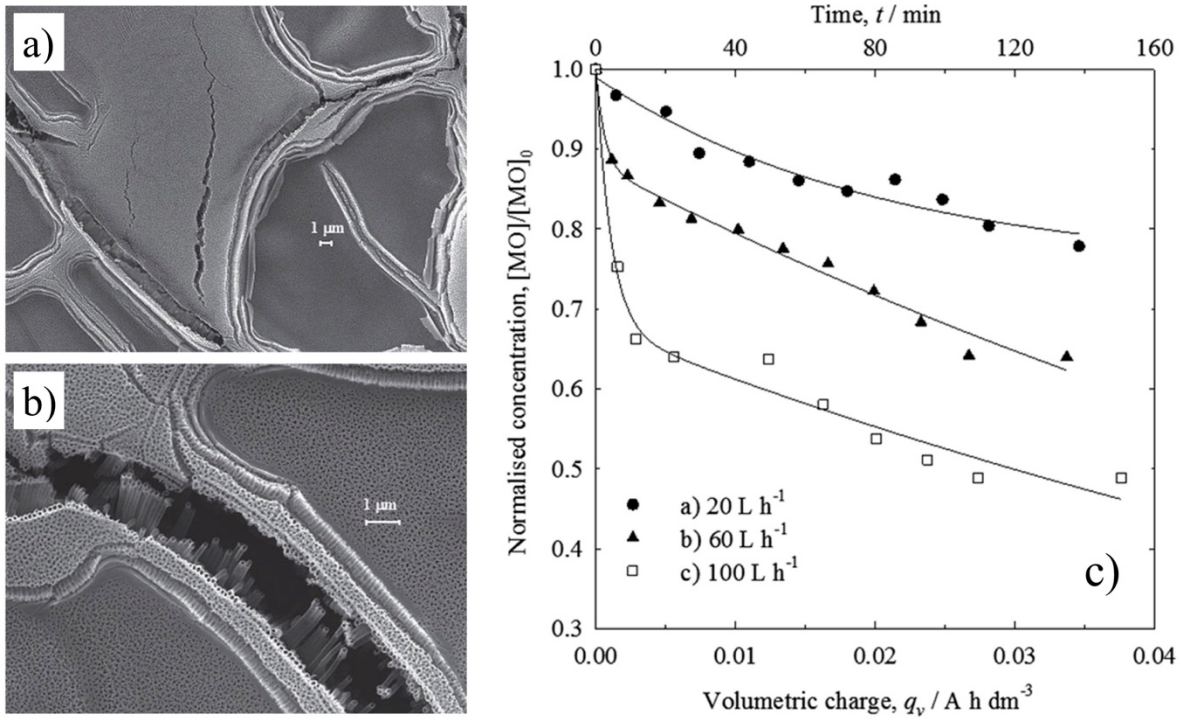

Figure 14. Anodic photocatalytic oxidation for removal of methyl orange (MO) at TiO_2 nanotubular arrays on planar titanium. SEM images of Ti plate anodised in 0.1 mol dm^{-3} NH_4F in a mixture of 2% vol. water in ethylene glycol: a) TiO_2 at different regions of the plate, b) close view of the nanotubes near a crevice. Cell potential of 40 V, heat treatment temperature, 450 ^oC for 100 min. c) Effect of volumetric charge on the oxidation of methyl orange under irradiation by light of 500 nm wavelength. 0.25 mmol dm^{-3} methyl orange in 0.1 mol dm^{-3} Na_2SO_4 at 15 ^oC and an electrode potential of 1.5 V *vs*. Ag/AgCl. Volumetric flow rate of electrolyte: (*) 20 L h^{-1}, (▲) 60 L h^{-1}, (□) 100 L h^{-1}, corresponding to mean linear flow velocities of 4.6, 13.2 and 23 cm s^{-1}. Adapted from de Vidales *et al.*,[50] with permission from Wiley.

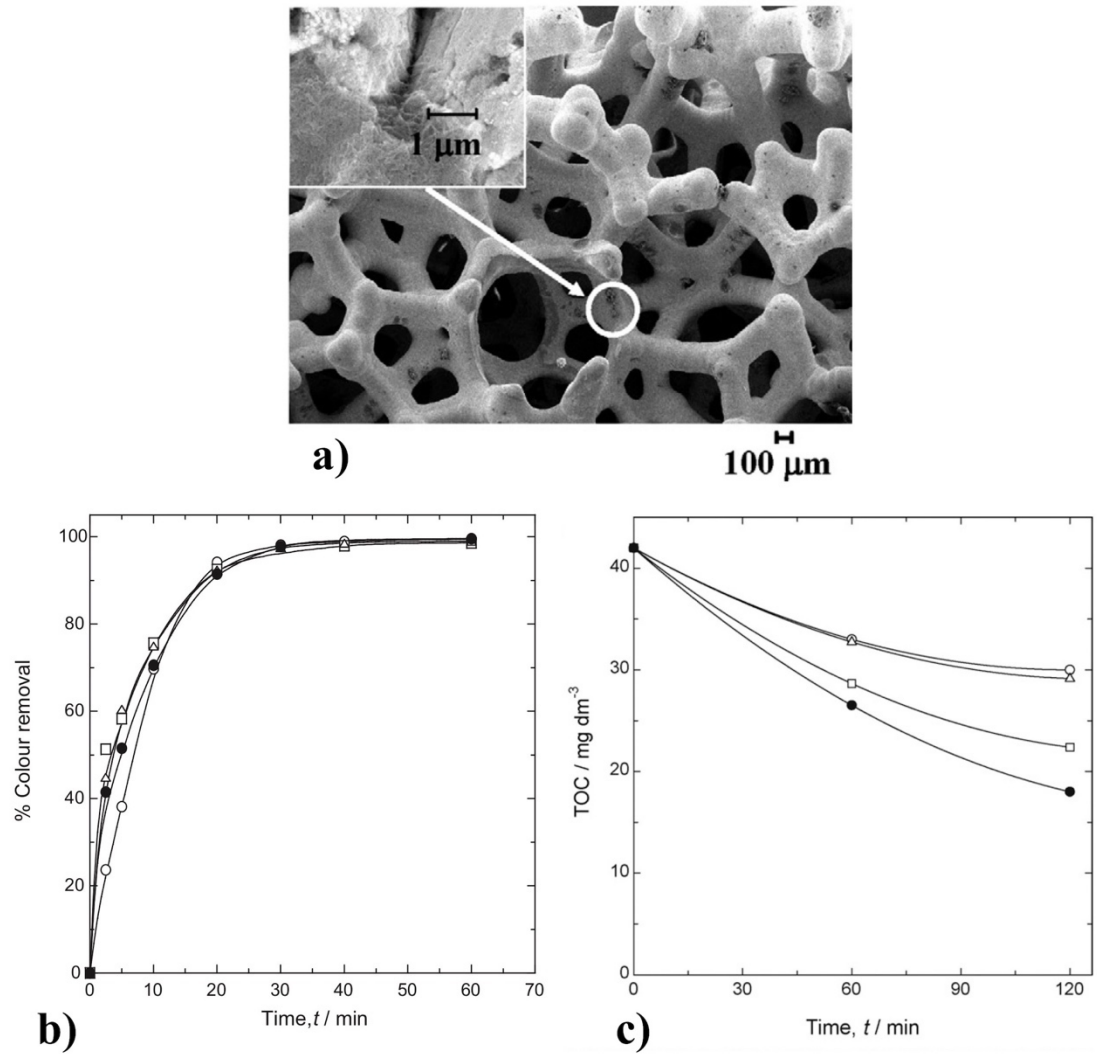

Figure 15. Electrochemical Fenton oxidation of methyl orange at a nanostructured PbO_2 deposit on carbon felt support. a) SEM image of a PbO_2/TiNT coating on RVC prepared at 2.5 A for 30 min. in a solution of 1.0 mol dm^{-3} $Pb(CH_3SO_3)_2$, 0.2 mol dm^{-3} MSA and 26 mmol dm^{-3} thiourea at 60 ◦C. b) Colour removal as a function of electrolysis time for a solution containing 0.25 mmol dm^{-3} methyl orange and 0.05 mol dm^{-3} Na_2SO_4 (pH 3.0) at 22.5 ºC employing a Ni plate cathode. Anodic oxidation with: ●,) ○) RVC/PbO_2 and □), △) RVC/PbO_2/TiNT. c) TOC removal as a function of time for the same experiments. Adapted from *Electrochimica Acta*, **56**(14), Recio FJ, Herrasti P, Sires I, Kulak AN, Bavykin DV, Ponce de León C, Walsh FC, The preparation of PbO_2 coatings on reticulated vitreous carbon for the electro-oxidation of organic pollutants, 5158–5165, Copyright (2011),[51] with permission from Elsevier.

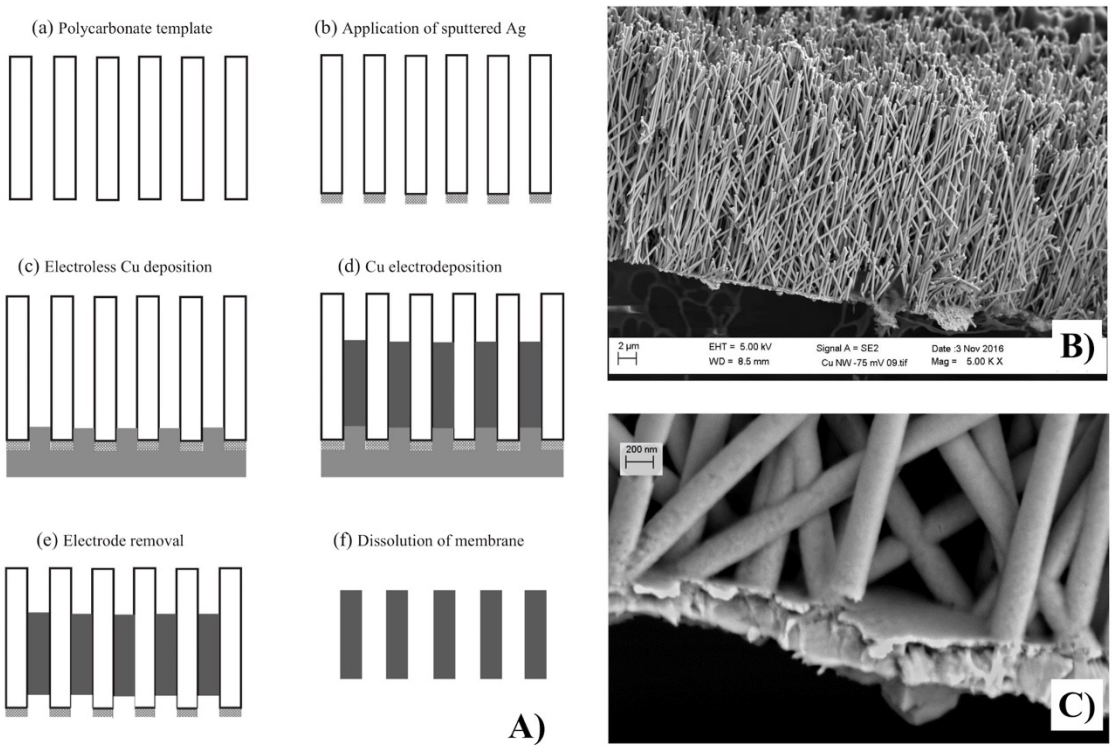

Figure 16. A copper nanowire forest grown by electroless deposition through a regular polycarbonate template. A) the steps involved in the deposition process, B) a scanning electron micrograph showing multiple nanowires after removal of the template and C) a closer view of B). Adapted from *Electrochemistry Communications*, 87, Graves J, Bowker ME, Summer A, Greenwood A, Ponce de León C, Walsh FC, A new procedure for the template synthesis of metal nanowires, 58–62, Copyright (2018),[53] with permission from Elsevier.

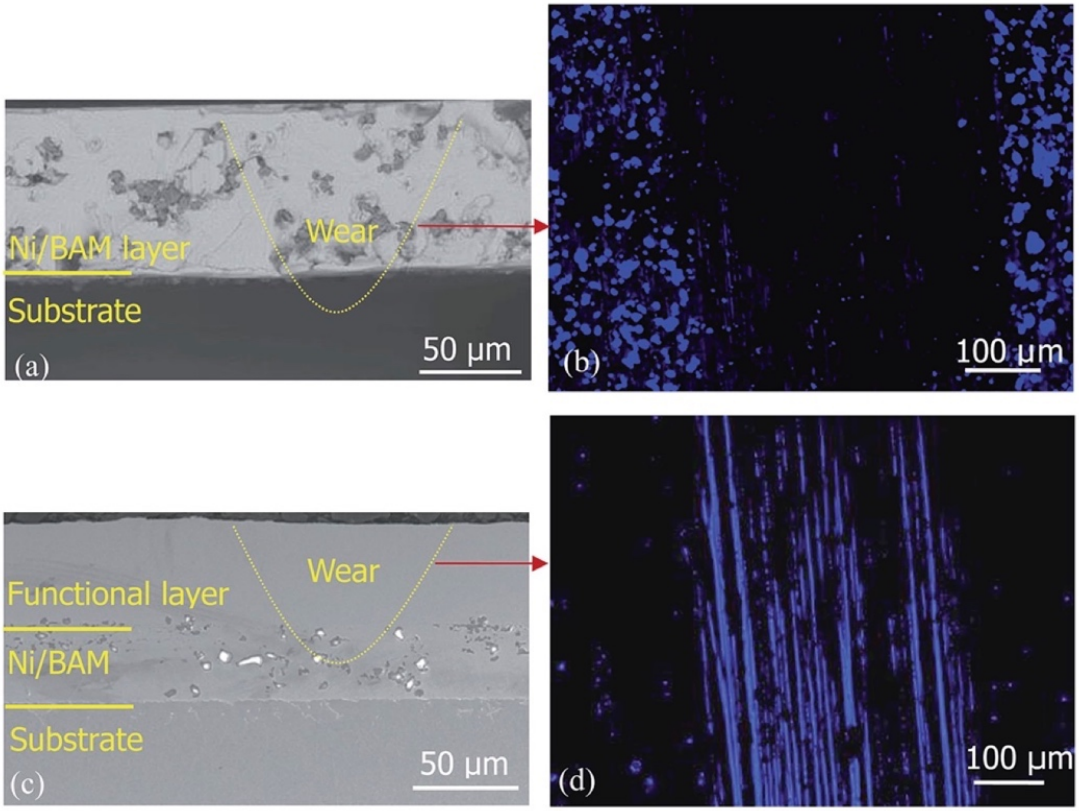

Figure 17. A composite, superhydrophobic coating incorporating *in-situ* wear diagnosis. a) Optical cross-section of a coating of luminescent particles on a mild steel substrate. b) Wear shown by fluorescent microscopy using light excitation at 450 nm shows. c) Optical cross-section of double coating having luminescent particles as an intermediate layer. d) Wear is revealed under photoluminescence when the intermediate later is exposed. Reproduced from He *et al.*,[58] with permission from The Royal Society of Chemistry.

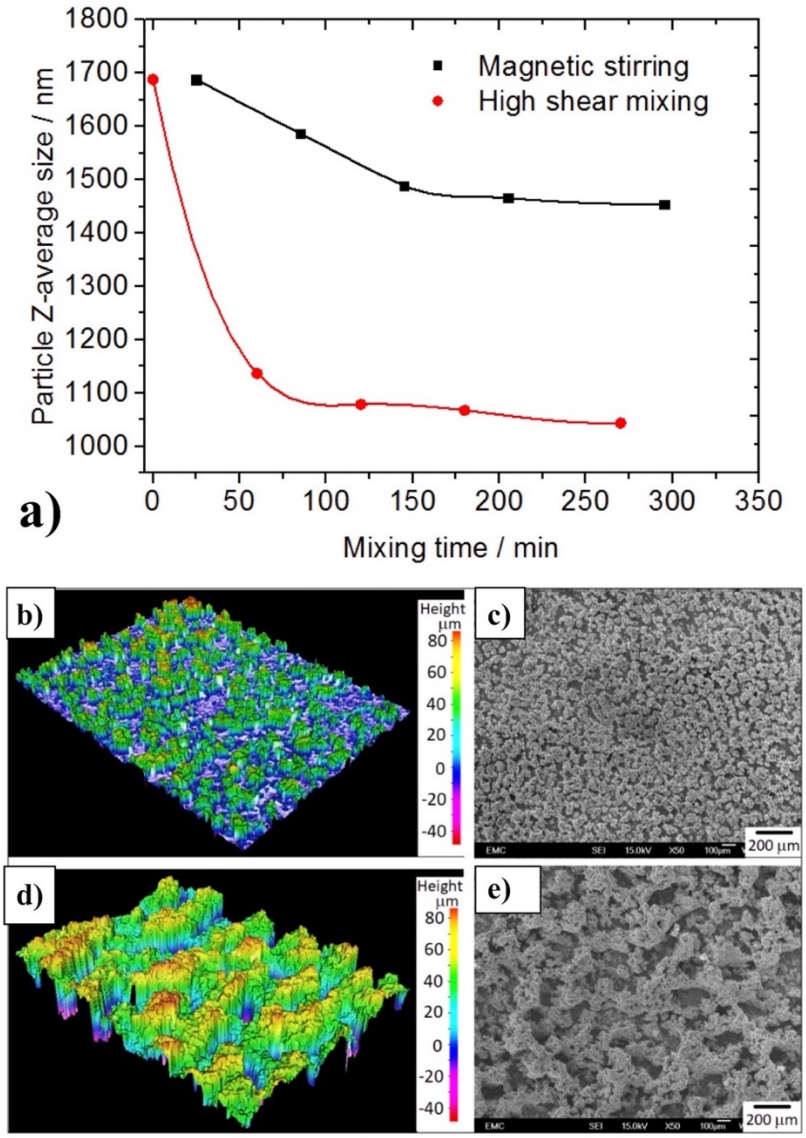

Figure 18. The importance of particle dispersion in the electrolyte for composite electrodeposition. a) MoS_2 particle Z-average size as a function of mixing time, as measured by an optical scattering particle measurement Zetasizer. 3D optical scan and SEM images of b), c): Ni-MoS_2 coating from an electrolyte in which particles were dispersed by high-shear mixing; d), e): Ni-MoS_2 electrodeposits from an electrolyte in which particles were dispersed by magnetic stirring.[59]

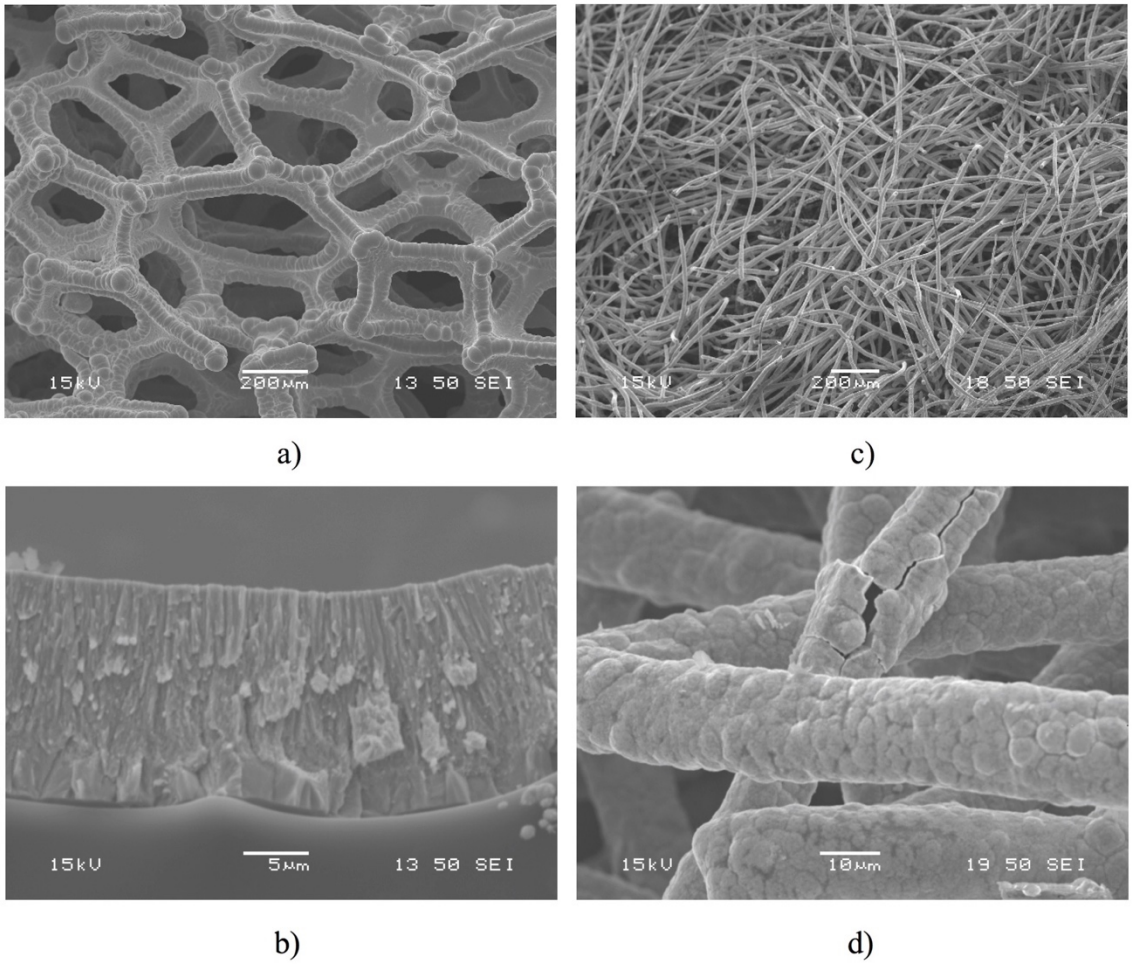

Figure 19. Electrodeposition of tin–copper alloys on porous, 3D supports. a) On 100 ppi RVC substrate with a volumetric porosity of 97%; b) closer, cross-sectional view of a modified 100 ppi RVC strut; c) On carbon felt with a volumetric porosity of 68% and fibre diameters between 5 and 10 μm; d) closer view of tin-copper coated felt fibres. Reproduced from Low *et al*.[60]

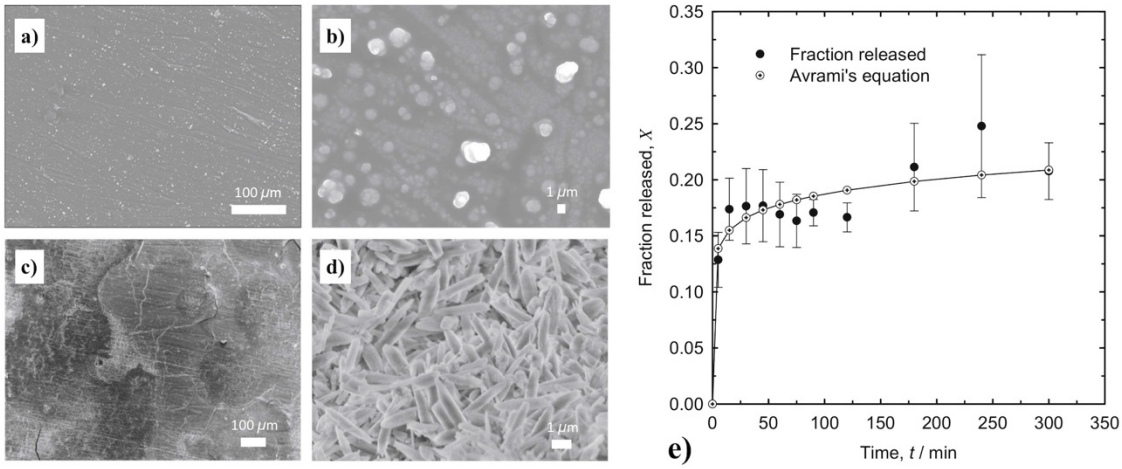

Figure 20. An example of controlled drug delivery. a), b) SEM images of the surface morphology of polypyrrole on a AZ31 alloy prepared in presence of sodium salicylate; c), d) SEM image of polypyrrole film having adsorbed ibuprofen. e) Ibuprofen release in terms of mass fraction from an 1 cm^2 electrode in 0.9 wt.% NaCl at 25 ^oC. Adapted from Alshammary *et al.* with permission from Springer (CC 4.0 licence).[62]